

# On the Compact Discontinuous Galerkin method for polytopal meshes

Mattia Corti<sup>\*†</sup> 

Sergio Gómez<sup>‡§</sup> 

## Abstract

The Compact Discontinuous Galerkin method was introduced by Peraire and Persson in (SIAM J. Sci. Comput., 30, 1806–1824, 2008). In this work, we present the stability and convergence analysis for the  $hp$ -version of this method applied to elliptic problems on polytopal meshes. Moreover, we introduce fast and practical algorithms that allow the CDG, LDG, and BR2 methods to be implemented within a unified framework. Our numerical experiments show that the CDG method yields a compact stencil for the stiffness matrix, with faster assembly and solving times compared to the LDG and BR2 methods. We numerically study how coercivity depends on the method parameters for various mesh types, with particular focus on the number of facets per mesh element. Finally, we demonstrate the importance of choosing the correct directions for the numerical fluxes when using variable polynomial degrees.

**Keywords.** Compact Discontinuous Galerkin method;  $hp$  error analysis; polytopal meshes

**Mathematics Subject Classification.** 65N30, 65N12, 65N15

## 1 Introduction

In this work, we study some theoretical and computational aspects of the Compact Discontinuous Galerkin (CDG) method for elliptic problems on polytopal meshes. The CDG method was first introduced by Peraire and Persson in [27] and combines features of the Local Discontinuous Galerkin (LDG) method proposed by Cockburn and Shu [18], and of the modified version of the Bassi–Rebay method (BR2) in [7]. The CDG method has also been analyzed for nonlinear convection–diffusion problems [9] and nearly incompressible linear elasticity models [23]. In addition, geometric multigrid solvers for the CDG method were investigated in [25].

The most attractive feature of the CDG method is that, due to its *built-in stabilization*, it shares the outstanding stability properties of the LDG method while recovering a *compact stencil* similar to that of the BR2 method, i.e., only the degrees of freedom (DoFs) belonging to neighboring elements are connected in the discretization. Such a compact stencil is typical of methods formulated directly for the primal variable, e.g., the interior-penalty discontinuous Galerkin (IPDG) [4] and the direct discontinuous Galerkin (DDG) [24] methods. In contrast, in the LDG framework, an arbitrary choice of the weighted-average parameters in the definition of the numerical fluxes may lead to a *full stencil*, involving not only immediate neighbors but also their neighbors (see [30, §3.3] and [14, §4.1]). In [15], some heuristic algorithms were studied to determine suitable choices of the numerical fluxes that reduce the stencil of the LDG method for simplicial meshes. However, the discussion in [15] makes it clear that a compact stencil cannot be achieved for arbitrary unstructured meshes. Finally, the CDG method shares the characteristic feature of the LDG method of using weighted averages in the definition of the numerical fluxes, which allows for a reduction of the interface integrals to compute, saving computational cost of assembling the stiffness matrix compared to the BR2 method. This is of particular interest when agglomerated meshes with a large number of facets for each element are considered (see [3, 6]).

<sup>\*</sup>Faculty of Mathematics, University of Vienna, Oskar-Morgenstern-Platz 1, Vienna, 1090, Austria

<sup>†</sup>MOX-Dipartimento di Matematica, Politecnico di Milano, Piazza Leonardo da Vinci 32, Milan, 20133, Italy ([mat-tia.corti@polimi.it](mailto:mat-tia.corti@polimi.it))

<sup>‡</sup>Department of Mathematics and Applications, University of Milano-Bicocca, Via Cozzi 55, 20125 Milan, Italy ([sergio.gomezmacias@unimib.it](mailto:sergio.gomezmacias@unimib.it))

<sup>§</sup>IMATI-CNR “E. Magenes”, Via Ferrata 5, 27100 Pavia, Italy

The stencil of a method directly impacts both computational efficiency and memory requirements. A reduction of the stencil is particularly relevant for polytopal meshes, where each element may have several neighbors, which can lead to a dramatic increase in the density of the associated matrices. In recent decades, there has been a steadily growing interest in numerical methods designed to handle polytopal meshes, as they allow for a more efficient approximation of complex geometries or interfaces. Such a class includes the virtual element method (VEM) [8], the Hybrid High-Order (HHO) method [20], and discontinuous Galerkin (DG) methods [12, 13, 34].

In this work, we focus on DG methods, which have the advantage that the number of DoFs is independent of the geometry of the elements.

**Model problem.** Let  $\Omega \subset \mathbb{R}^d$  ( $d \in \{2, 3\}$ ) be an open, bounded domain with Lipschitz boundary  $\partial\Omega = \Gamma_D \cup \Gamma_N$ , where  $\Gamma_D$  and  $\Gamma_N$  are disjoint sets ( $\Gamma_D \cap \Gamma_N = \emptyset$ ) and denote the parts of the boundary of  $\Omega$  where Dirichlet and Neumann boundary conditions are imposed, respectively. We further assume that  $\Gamma_D$  has strictly positive  $(d-1)$ -dimensional measure.

Given a symmetric diffusion tensor  $\kappa \in L^\infty(\Omega)^{d \times d}$  with

$$k^* := \|\kappa\|_{L^\infty(\Omega)^{d \times d}} \quad \text{and} \quad k_* := \operatorname{ess\,inf}_{\mathbf{x} \in \Omega} \lambda_{\min}(\kappa(\mathbf{x})) > 0, \quad (1.1)$$

a source term  $f \in L^2(\Omega)$ , a Dirichlet datum  $g_D \in H^{1/2}(\Gamma_D)$ , and a Neumann datum  $g_N \in L^2(\Gamma_N)$ , we consider the following boundary value problem (BVP): find  $u : \Omega \rightarrow \mathbb{R}$  such that

$$-\nabla \cdot (\kappa \nabla u) = f \quad \text{in } \Omega, \quad (1.2a)$$

$$u = g_D \quad \text{on } \Gamma_D, \quad (1.2b)$$

$$\kappa \nabla u \cdot \mathbf{n}_\Omega = g_N \quad \text{on } \Gamma_N, \quad (1.2c)$$

where  $\mathbf{n}_\Omega$  is the unit normal vector pointing outward  $\Omega$ . We recall that, since  $g_D \in H^{1/2}(\Gamma_D)$ , there exists a unique continuous weak solution  $u$  to (1.2) that belongs to the convex space  $H_{\Gamma_D} := \{\phi \in H^1(\Omega) : \phi = g_D \text{ on } \Gamma_D\}$ .

**Novelty.** To the best of our knowledge, this is the first work in which the following aspects of the CDG method have been studied.

- We describe the CDG method for variable degrees of approximation and fairly general polytopal meshes.
- We show that the method is well posed without requiring a further stabilization term provided that the weighted averages in the definition of the numerical fluxes satisfy Assumption 2.1 below.
- We derive *hp-a priori* error estimates in the energy norm, where we employ the recent approximation results from [22].
- We discuss how the CDG, LDG, and BR2 methods can be implemented within a unified framework, where the stiffness matrix is assembled without relying on large auxiliary matrices.

**Notations.** We shall use the standard notation for Sobolev spaces. Given an open set  $\Upsilon \subset \mathbb{R}^d$  ( $d = 2, 3$ ) and  $s > 0$ , we denote by  $H^s(\Upsilon)$  the corresponding Sobolev space with seminorm  $|\cdot|_{H^s(\Upsilon)}$  and norm  $\|\cdot\|_{H^s(\Upsilon)}$ . We also denote by  $L^2(\Upsilon)$  the space of Lebesgue square integrable functions in  $\Upsilon$  with norm  $\|\cdot\|_{L^2(\Upsilon)}$ . A superscript  $d$  will be used to identify the spaces of  $d$ -vector-valued functions.

**Outline.** The remainder of the paper is organized as follows: Section 2 presents the standard notation on polytopal meshes and the CDG method. Moreover, the existence of a discrete solution is proven in Section 2.4. In Section 3, we derive an *a-priori* error estimate, while Section 4 discusses computational aspects and describes fast algorithms for the CDG, LDG, and BR2 methods. In Section 5, we carry out some numerical experiments aimed at validating our theoretical results and comparing the CDG method with the LDG and BR2 methods in terms of computational efficiency and stiffness matrix properties. Finally, in Section 6, we draw some conclusions and discuss future developments.

## 2 Description of the method

In Section 2.1, we introduce some notation for polytopal meshes and some standard DG operators. The CDG method is described in Section 2.2, and the reduced formulation used in the analysis is derived in Section 2.3. Finally, the existence of a discrete solution is proven in Section 2.4.

### 2.1 Polytopal meshes and DG notations

Let  $\{\Omega_h\}_{h>0}$  be a family of polytopal partitions of  $\Omega$ , where the subscript  $h$  stands for the meshsize of  $\Omega_h$ . More precisely, we set  $h := \max_{K \in \Omega_h} h_K$ , where  $h_K$  denotes the diameter of the element  $K \in \Omega_h$ . We call “mesh facets” the  $(d-1)$ -dimensional facets with positive measure lying on a  $(d-1)$ -dimensional hyperplane that compose either the nonempty intersection  $K_1 \cap K_2$  for two elements  $K_1, K_2 \in \Omega_h$ , or the nonempty intersection  $K \cap \partial\Omega$  for  $K \in \Omega_h$ . The set of mesh facets of  $\Omega_h$  is denoted by  $\mathcal{F}_h = \mathcal{F}_h^{\mathcal{I}} \cup \mathcal{F}_h^{\mathcal{D}} \cup \mathcal{F}_h^{\mathcal{N}}$ , where  $\mathcal{F}_h^{\mathcal{I}}$  is the set of interior facets of  $\Omega_h$ , and  $\mathcal{F}_h^{\mathcal{D}}$  and  $\mathcal{F}_h^{\mathcal{N}}$  are the sets of facets lying on  $\Gamma_D$  and  $\Gamma_N$ , respectively. For each  $F \in \mathcal{F}_h^{\mathcal{I}}$ , let  $\mathbf{n}_F$  denote one of the two  $d$ -dimensional unit normal vectors to  $F$ . Moreover, for each  $F \in \mathcal{F}_h^{\mathcal{D}} \cup \mathcal{F}_h^{\mathcal{N}}$ , we set  $\mathbf{n}_F := \mathbf{n}_\Omega$ . Finally, we denote by  $\mathcal{F}_K$  and  $\mathcal{N}_K$  the sets of facets and neighbors of  $K$ , respectively.

Let  $\mathbf{p} = (p_K)_{K \in \Omega_h}$  be a vector that assigns a degree of approximation  $p_K \geq 1$  to each element  $K \in \Omega_h$ . We define the following piecewise polynomial spaces:

$$\mathcal{V}_h^{\mathbf{p}} := \prod_{K \in \Omega_h} \mathcal{P}^{p_K}(K) \quad \text{and} \quad \mathcal{M}_h^{\mathbf{p}} := \prod_{K \in \Omega_h} \mathcal{P}^{p_K}(K)^d,$$

where  $\mathcal{P}^{p_K}(K)$  denotes the space of polynomials defined on  $K$  of degree at most  $p_K$ . We further define the following broken Sobolev spaces: given  $s > 0$ ,

$$H^s(\Omega_h) := \{\phi \in L^2(\Omega) : \phi|_K \in H^s(K) \text{ for all } K \in \Omega_h\}.$$

We employ standard notation for weighted averages ( $\{\!\!\{ \cdot \}\!\!\}_{\alpha_F}$ ) and normal jumps ( $[\![ \cdot ]\!]_N$ ) of piecewise smooth scalar-valued ( $v$ ) and  $d$ -vector-valued ( $\mathbf{r}$ ) functions: given a facet  $F \in \mathcal{F}_h^{\mathcal{I}}$  shared by two elements  $K_1$  and  $K_2$  in  $\Omega_h$  with  $\mathbf{n}_F = \mathbf{n}_{K_1}$ , and a prescribed weighted-average parameter  $\alpha_F \in [0, 1]$ , we define

$$\begin{aligned} \{\!\!\{ v \}\!\!\}_{\alpha_F} &:= (1 - \alpha_F)v|_{K_1} + \alpha_F v|_{K_2}, & [\![ v ]\!]_N &:= (v|_{K_1} - v|_{K_2})\mathbf{n}_F, \\ \{\!\!\{ \mathbf{r} \}\!\!\}_{1-\alpha_F} &:= \alpha_F \mathbf{r}|_{K_1} + (1 - \alpha_F) \mathbf{r}|_{K_2}, & [\![ \mathbf{r} ]\!]_N &:= (\mathbf{r}|_{K_1} - \mathbf{r}|_{K_2}) \cdot \mathbf{n}_F. \end{aligned}$$

We define the local lifting operator  $\mathcal{L}^F : L^2(F)^d \rightarrow \mathcal{M}_h^{\mathbf{p}}$  as follows:

$$\int_{\Omega} \mathcal{L}^F(\phi) \cdot \mathbf{r}_h \, dx = \int_F \phi \cdot \{\!\!\{ \mathbf{r}_h \}\!\!\}_{1-\alpha_F} \, dS \quad \forall \mathbf{r}_h \in \mathcal{M}_h^{\mathbf{p}}. \quad (2.1)$$

Similarly, for each boundary facet  $F \in \mathcal{F}_h^{\mathcal{D}}$ , we define the local lifting operator  $\mathcal{L}_{\mathcal{D}}^F : L^2(F) \rightarrow \mathcal{M}_h^{\mathbf{p}}$  as

$$\int_{\Omega} \mathcal{L}_{\mathcal{D}}^F(\phi) \cdot \mathbf{r}_h \, dx = \int_F \phi \mathbf{r}_h \cdot \mathbf{n}_\Omega \, dS \quad \forall \mathbf{r}_h \in \mathcal{M}_h^{\mathbf{p}}. \quad (2.2)$$

Moreover, we define the global lifting operators  $\mathcal{L}_h^{\mathcal{D}} : H^{1/2+\varepsilon}(\Omega_h) \rightarrow \mathcal{M}_h^{\mathbf{p}}$  and  $\mathcal{L}_h : H^{1/2+\varepsilon}(\Omega_h) \rightarrow \mathcal{M}_h^{\mathbf{p}}$  with  $\varepsilon > 0$  by

$$\mathcal{L}_h^{\mathcal{D}} v_h := \sum_{F \in \mathcal{F}_h^{\mathcal{D}}} \mathcal{L}_{\mathcal{D}}^F(v_h|_F) \quad \text{and} \quad \mathcal{L}_h v_h := \sum_{F \in \mathcal{F}_h^{\mathcal{I}}} \mathcal{L}^F([\![ v_h ]\!]_N) + \mathcal{L}_h^{\mathcal{D}} v_h. \quad (2.3)$$

We further denote by  $\mathbf{\Pi}_h : L^2(\Omega)^d \rightarrow \mathcal{M}_h^{\mathbf{p}}$  the  $L^2(\Omega)^d$ -orthogonal projection operator onto  $\mathcal{M}_h^{\mathbf{p}}$ , and by  $\nabla_h : H^1(\Omega_h) \rightarrow L^2(\Omega)^d$  the piecewise gradient operator defined on  $\Omega_h$ . Finally, we shall use the following short-hand notation for sums of integrals over the facets of  $\Omega_h$ : for  $\star \in \{\mathcal{I}, \mathcal{D}, \mathcal{N}\}$ ,

$$\int_{\mathcal{F}_h^{\star}} \phi \, dS := \sum_{F \in \mathcal{F}_h^{\star}} \int_F \phi \, dS.$$

## 2.2 Compact discontinuous Galerkin method

In the spirit of [28] (see also [27, §2.2]), we introduce the auxiliary variables  $\mathbf{q} = -\nabla u$  and  $\boldsymbol{\sigma} = \kappa \mathbf{q}$ , and rewrite model (1.2) as follows:

$$\begin{aligned}\mathbf{q} &= -\nabla u && \text{in } \Omega, \\ \boldsymbol{\sigma} &= \kappa \mathbf{q} && \text{in } \Omega, \\ \nabla \cdot \boldsymbol{\sigma} &= f && \text{in } \Omega, \\ u &= g_D && \text{on } \Gamma_D, \\ \boldsymbol{\sigma} \cdot \mathbf{n}_\Omega &= -g_N && \text{on } \Gamma_N.\end{aligned}$$

As in the unified framework of DG methods in [5], we consider the following discrete variational formulation: find  $(u_h, \mathbf{q}_h, \boldsymbol{\sigma}_h) \in \mathcal{V}_h^p \times \mathcal{M}_h^p \times \mathcal{M}_h^p$  such that, for each element  $K \in \Omega_h$ , there hold

$$\int_K \mathbf{q}_h \cdot \mathbf{r}_h \, dx = - \int_{\partial K} \hat{u}_h \mathbf{r}_h \cdot \mathbf{n}_K \, dS + \int_K u_h \nabla \cdot \mathbf{r}_h \, dx \quad \forall \mathbf{r}_h \in \mathcal{M}_h^p, \quad (2.4a)$$

$$\int_K \boldsymbol{\sigma}_h \cdot \mathbf{s}_h \, dx = \int_K \kappa \mathbf{q}_h \cdot \mathbf{s}_h \, dx \quad \forall \mathbf{s}_h \in \mathcal{M}_h^p, \quad (2.4b)$$

$$\int_{\partial K} v_h \hat{\boldsymbol{\sigma}}_h \cdot \mathbf{n}_K \, dS - \int_K \boldsymbol{\sigma}_h \cdot \nabla v_h \, dx = \int_K f v_h \, dx \quad \forall v_h \in \mathcal{V}_h^p, \quad (2.4c)$$

where the *numerical fluxes*  $\hat{u}_h$  and  $\hat{\boldsymbol{\sigma}}_h$  are approximations of the traces of  $u$  and  $\boldsymbol{\sigma}$  on  $\mathcal{F}_h$ , and they characterize the DG method.

For the CDG method (see [27, §3]), we define the numerical fluxes on each facet  $F \in \mathcal{F}_h$  as

$$\hat{u}_h := \begin{cases} \{u_h\}_{\alpha_F} & \text{if } F \in \mathcal{F}_h^I, \\ g_D & \text{if } F \in \mathcal{F}_h^D, \\ u_h & \text{if } F \in \mathcal{F}_h^N, \end{cases} \quad \hat{\boldsymbol{\sigma}}_h := \begin{cases} \{\boldsymbol{\sigma}_h^F\}_{1-\alpha_F} & \text{if } F \in \mathcal{F}_h^I, \\ \boldsymbol{\sigma}_h^F & \text{if } F \in \mathcal{F}_h^D, \\ -g_N \mathbf{n}_\Omega & \text{if } F \in \mathcal{F}_h^N, \end{cases} \quad (2.5)$$

where  $\boldsymbol{\sigma}_h^F \in \mathcal{M}_h^p$  is an auxiliary function defined below and, for each  $F \in \mathcal{F}_h^I$ , the weighted-average parameter  $\alpha_F$  is either 0 or 1.

For variable degrees of approximation, the choice  $\alpha_F \in \{0, 1\}$ , which corresponds to choosing a one-sided trace, leads to the following assumption.

**Assumption 2.1** (Weighted-average parameters). *For any interior facet  $F \in \mathcal{F}_h^I$  shared by two elements  $K_1$  and  $K_2$  in  $\Omega_h$  with  $p_{K_1} > p_{K_2}$ , the weight parameter  $\alpha_F$  is chosen such that*

$$\{\boldsymbol{\sigma}_h^F\}_{1-\alpha_F} = \boldsymbol{\sigma}_h^F|_{K_1}.$$

*More precisely, for neighboring elements with different degrees of approximation, we set  $\alpha_F$  so that the trace of  $\boldsymbol{\sigma}_h^F$  is taken from the element with higher degree.*

The previous assumption is made to guarantee the coercivity of the bilinear form of the CDG method (see Lemma 2.8 and Section 5.4 below). Consequently, for each  $K \in \Omega_h$ , we define

$$\mathcal{F}_K^{\text{out}} := \{F \in \mathcal{F}_K : F \in \mathcal{F}_h^I \text{ and } \{\cdot\}_{1-\alpha_F} = (\cdot)|_K\} \cup \{F \in \mathcal{F}_K : F \in \mathcal{F}_h^D\}, \quad (2.6)$$

$$\mathcal{N}_K^{\text{out}} := \{\tilde{K} \in \Omega_h : \mathcal{F}_K^{\text{out}} \cap \mathcal{F}_{\tilde{K}} \neq \emptyset\}, \quad (2.7)$$

In other words,  $\mathcal{F}_K^{\text{out}}$  is the set of facets of  $K$  such that the support of  $\mathcal{L}^F(\cdot)$  or  $\mathcal{L}_D^F(\cdot)$  is  $K$ . In addition, for each  $F \in \mathcal{F}_h^I \cup \mathcal{F}_h^D$ , we denote by  $K_F \in \Omega_h$  the only element such that  $F \in \mathcal{F}_{K_F}^{\text{out}}$ , and set

$$\nu_F^{\text{out}} := \text{card}(\mathcal{F}_{K_F}^{\text{out}}). \quad (2.8)$$

These definitions are illustrated in Figure 1.

As for the auxiliary local functions  $\boldsymbol{\sigma}_h^F \in \mathcal{M}_h^p$ , we first assign a parameter  $\chi_F > 0$  to each facet  $F \in \mathcal{F}_h^I \cup \mathcal{F}_h^D$ . Then, for each interior facet  $F \in \mathcal{F}_h^I$ , we define  $\boldsymbol{\sigma}_h^F$  as the solution to the following local problem:

$$\begin{aligned}\int_\Omega \boldsymbol{\sigma}_h^F \cdot \mathbf{r}_h \, dx &= - \int_\Omega \kappa \nabla_h u_h \cdot \mathbf{r}_h \, dx + \chi_F \int_F [\![u_h]\!]_N \cdot \{\Pi_h(\kappa \mathbf{r}_h)\}_{1-\alpha_F} \, dS \\ &= - \int_\Omega \kappa (\nabla_h u_h - \chi_F \mathcal{L}^F([\![u_h]\!]_N)) \cdot \mathbf{r}_h \, dx \quad \forall \mathbf{r}_h \in \mathcal{M}_h^p.\end{aligned} \quad (2.9)$$

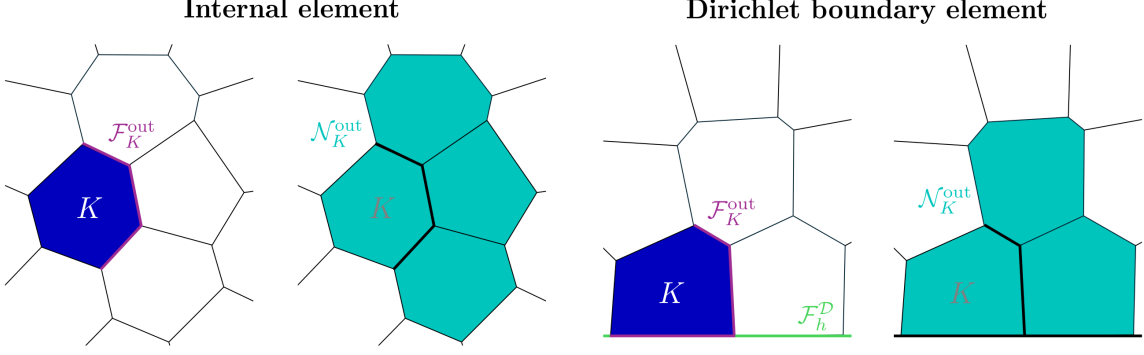


**Figure 1:** Schematic representation of the sets  $\mathcal{F}_K^{\text{out}}$  (purple on the left) and  $\mathcal{N}_K^{\text{out}}$  (light blue on the right) assuming  $\alpha_F = 1$  for  $\beta_F = \mathbf{n}_F \cdot [1, 0]^T \geq 1$ . Internal element case (left panel) and Dirichlet boundary element case (right panel).

Analogously, for each boundary facet  $F \in \mathcal{F}_h^{\mathcal{D}}$ ,  $\boldsymbol{\sigma}_h^F \in \mathcal{M}_h^p$  is defined as the solution to

$$\begin{aligned} \int_{\Omega} \boldsymbol{\sigma}_h^F \cdot \mathbf{r}_h \, dx &= - \int_{\Omega} \boldsymbol{\kappa} \nabla_h u_h \cdot \mathbf{r}_h \, dx + \chi_F \int_F (u_h - g_D) \boldsymbol{\Pi}_h(\boldsymbol{\kappa} \mathbf{r}_h) \cdot \mathbf{n}_{\Omega} \, dS \\ &= - \int_{\Omega} \boldsymbol{\kappa} (\nabla_h u_h - \chi_F \mathcal{L}_D^F(u_h|_F - g_D)) \cdot \mathbf{r}_h \, dx \quad \forall \mathbf{r}_h \in \mathcal{M}_h^p. \end{aligned} \quad (2.10)$$

Therefore, from (2.9) and (2.10), we can deduce the following expressions for  $\boldsymbol{\sigma}_h^F$ :

$$\boldsymbol{\sigma}_h^F = \begin{cases} -\boldsymbol{\Pi}_h(\boldsymbol{\kappa}(\nabla_h u_h - \chi_F \mathcal{L}_D^F([u_h]_N))) & \text{if } F \in \mathcal{F}_h^{\mathcal{I}}, \\ -\boldsymbol{\Pi}_h(\boldsymbol{\kappa}(\nabla_h u_h - \chi_F \mathcal{L}_D^F(u_h|_F - g_D))) & \text{if } F \in \mathcal{F}_h^{\mathcal{D}}. \end{cases} \quad (2.11)$$

We make the following additional assumption on the parameters  $\chi_F$ , which we use in Lemma 2.7 to show that the seminorm induced by the bilinear form of the CDG method is a norm in  $\mathcal{V}_h^p$ .

**Assumption 2.2** (Choice of  $\chi_F$ ). *We assume that there is a positive constant  $\gamma$  independent of  $h$  such that*

$$0 < \frac{\nu_F^{\text{out}}}{\chi_F} \leq \gamma < 1 \quad \forall F \in \mathcal{F}_h^{\mathcal{I}} \cup \mathcal{F}_h^{\mathcal{D}},$$

where  $\nu_F^{\text{out}}$  is the constant defined in (2.8).

**Remark 2.3** (Relation with the LDG method). *The LDG method is obtained by modifying the definition of the numerical flux  $\hat{\boldsymbol{\sigma}}_h$  as follows:*

$$\hat{\boldsymbol{\sigma}}_h := \begin{cases} \{\{\boldsymbol{\sigma}_h\}_{1-\alpha_F} + \eta_F [u_h]_N\} & \text{if } F \in \mathcal{F}_h^{\mathcal{I}}, \\ \boldsymbol{\sigma}_h + \eta_F (u_h - g_D) & \text{if } F \in \mathcal{F}_h^{\mathcal{D}}, \\ -g_N \mathbf{n}_{\Omega} & \text{if } F \in \mathcal{F}_h^{\mathcal{N}}, \end{cases}$$

where, for each  $F \in \mathcal{F}_h^{\mathcal{I}}$ ,  $\alpha_F \in [0, 1]$ , and the piecewise-constant stabilization function  $\eta_F \in L^{\infty}(\mathcal{F}_h^{\mathcal{I}} \cup \mathcal{F}_h^{\mathcal{D}})$  satisfies  $\eta_* := \text{ess inf}_{\mathcal{F}_h^{\mathcal{I}} \cup \mathcal{F}_h^{\mathcal{D}}} \eta_F > 0$ .

Analogously to as in (2.11), for the LDG method, the function  $\boldsymbol{\sigma}_h$  can be explicitly expressed as (see also equation (2.12) below)

$$\boldsymbol{\sigma}_h = -\boldsymbol{\Pi}_h(\boldsymbol{\kappa}(\nabla_h u_h - \mathcal{L}_h u_h + \mathcal{L}_h^D(g_D))).$$

The implicit dependence in the LDG method of the numerical flux  $\hat{\boldsymbol{\sigma}}_h$  on the global lifting  $\mathcal{L}_h u_h$  leads to a larger stencil.

The analysis of the LDG method on polytopal meshes was carried out in [35] (for the  $h$  version) and in [21] (for the  $hp$  version in a space-time setting).  $\blacksquare$

**Remark 2.4** (Relation with the BR2 method). *The BR2 method is obtained by setting  $\alpha_F = 1/2$  in (2.5) for all the internal facets  $F \in \mathcal{F}_h^{\mathcal{I}}$  (see [10, §3] and [6, §3.2]). For this choice of the weighted-average parameters, the support of  $\boldsymbol{\sigma}_h^F$  is the union of both elements sharing the facet  $F$ , which leads to an increase in the computational cost compared to the CDG method. Namely, for each internal face  $F$ , we need to compute two interface integrals instead of one.*

The analysis in [10, §IV] of the BR2 method was extended to agglomerated meshes in two-dimensional domains in [6, §3.3]. Assumption 2.2 on the choice of the parameters  $\chi_F$  is inspired by the one made in [6, Thm. 1], which allows for a milder dependence of the constants in the a priori error estimates on the maximum number of facets of the elements in  $\Omega_h$ . ■

**Remark 2.5** (The CDG2 version). An alternative version (CDG2) of the CDG method was introduced in [9] in the context of nonlinear convection–diffusion–reaction equations. For the model problem (1.2), it corresponds to the following choice of the numerical fluxes in the abstract variational formulation (2.4):

$$\begin{aligned}\widehat{u}_h &:= \begin{cases} \{u_h\}_{1/2} & \text{if } F \in \mathcal{F}_h^{\mathcal{I}}, \\ g_D & \text{if } F \in \mathcal{F}_h^{\mathcal{D}}, \\ u_h & \text{if } F \in \mathcal{F}_h^{\mathcal{N}}, \end{cases} \\ \widehat{\boldsymbol{\sigma}}_h &:= \begin{cases} -\{\Pi_h(\boldsymbol{\kappa} \nabla_h u_h)\}_{1/2} + \chi_F \{\Pi_h(\boldsymbol{\kappa} \mathcal{L}^F(\llbracket u_h \rrbracket_N))\}_{1-\alpha_F} & \text{if } F \in \mathcal{F}_h^{\mathcal{I}}, \\ -\Pi_h(\boldsymbol{\kappa} (\nabla_h u_h - \chi_F \mathcal{L}_D^F(u_h|_F - g_D)))|_F & \text{if } F \in \mathcal{F}_h^{\mathcal{D}}, \\ -g_N \mathbf{n}_\Omega & \text{if } F \in \mathcal{F}_h^{\mathcal{N}}, \end{cases}\end{aligned}$$

where, for each  $F \in \mathcal{F}_h^{\mathcal{I}}$ ,  $\alpha_F \in \{0, 1\}$ . Thus, this version considers standard (arithmetic) averages except for the term in the definition in (2.11) of  $\boldsymbol{\sigma}_h^F$  involving the local lifting  $\mathcal{L}^F(\llbracket u_h \rrbracket_N)$ . ■

**Remark 2.6** (Absence of a stabilization term). Motivated by [9, Thm. 2] for standard meshes, which states that it is not necessary to include a stability term in the CDG method if the parameters  $\chi_F$  are chosen appropriately, we have not introduced any stability term in the definition of  $\widehat{\boldsymbol{\sigma}}_h$  in (2.5) (cf. [27, §3] and [9, §2.1]). This allows us to avoid computing an additional discrete operator in the method. Moreover, the inclusion of a stability term would not solve the issue of the dependence of the error estimates on the maximum number of facets, unless the stability parameter were taken “large enough”, as in the IPDG method. ■

### 2.3 Reduced formulation

For the analysis, we proceed as in [27] and [9], by first rewriting the method as a variational problem involving only the scalar unknown  $u_h$ .

Summing (2.4a) over all the elements of the mesh  $\Omega_h$ , integrating by parts, and using the average–jump identity

$$\{v_h\}_{\alpha_F} \llbracket \mathbf{r}_h \rrbracket_N + \llbracket v_h \rrbracket_N \cdot \{ \mathbf{r}_h \}_{1-\alpha_F} = \llbracket v_h \mathbf{r}_h \rrbracket_N \quad \forall (v_h, \mathbf{r}_h) \in \mathcal{V}_h^p \times \mathcal{M}_h^p,$$

and the definition of the global lifting operators, we get

$$\begin{aligned}\int_{\Omega} \mathbf{q}_h \cdot \mathbf{r}_h \, dx &= \sum_{K \in \Omega_h} \int_K u_h \nabla \cdot \mathbf{r}_h \, dx - \int_{\mathcal{F}_h^{\mathcal{I}}} \{u_h\}_{\alpha_F} \llbracket \mathbf{r}_h \rrbracket_N \, dS - \int_{\mathcal{F}_h^{\mathcal{D}}} g_D \mathbf{r}_h \cdot \mathbf{n}_\Omega \, dS - \int_{\mathcal{F}_h^{\mathcal{N}}} u_h \mathbf{r}_h \cdot \mathbf{n}_\Omega \, dS \\ &= - \int_{\Omega} \nabla_h u_h \cdot \mathbf{r}_h \, dx + \int_{\mathcal{F}_h^{\mathcal{I}}} (\llbracket u_h \mathbf{r}_h \rrbracket_N - \{u_h\}_{\alpha_F} \llbracket \mathbf{r}_h \rrbracket_N) \, dS + \int_{\mathcal{F}_h^{\mathcal{D}}} (u_h - g_D) \mathbf{r}_h \cdot \mathbf{n}_\Omega \, dS \\ &= - \int_{\Omega} \nabla_h u_h \cdot \mathbf{r}_h \, dx + \int_{\mathcal{F}_h^{\mathcal{I}}} \llbracket u_h \rrbracket_N \cdot \{ \mathbf{r}_h \}_{1-\alpha_F} \, dS + \int_{\mathcal{F}_h^{\mathcal{D}}} (u_h - g_D) \mathbf{r}_h \cdot \mathbf{n}_\Omega \, dS \\ &= - \int_{\Omega} \nabla_h u_h \cdot \mathbf{r}_h \, dx + \sum_{F \in \mathcal{F}_h^{\mathcal{I}}} \int_{\Omega} \mathcal{L}^F(\llbracket u_h \rrbracket_N) \cdot \mathbf{r}_h \, dx + \sum_{F \in \mathcal{F}_h^{\mathcal{D}}} \int_{\Omega} \mathcal{L}_D^F(u_h|_F - g_D) \cdot \mathbf{r}_h \, dx \\ &= - \int_{\Omega} (\nabla_h u_h - \mathcal{L}_h u_h + \mathcal{L}_h^D(g_D)) \cdot \mathbf{r}_h \, dx,\end{aligned}$$

which leads to the following expressions for  $\mathbf{q}_h$  and  $\boldsymbol{\sigma}_h$ :

$$\mathbf{q}_h = -(\nabla_h u_h - \mathcal{L}_h u_h + \mathcal{L}_h^D(g_D)) \quad \text{and} \quad \boldsymbol{\sigma}_h = \boldsymbol{\Pi}_h(\boldsymbol{\kappa} \mathbf{q}_h). \quad (2.12)$$

Summing the left-hand side of (2.4c) over all the elements in  $\Omega_h$ , substituting the definition of the numerical flux  $\widehat{\boldsymbol{\sigma}}_h$  in (2.5), and using the identities in (2.12), the expressions in (2.11) for  $\boldsymbol{\sigma}_h^F$ , and the

definition of the local and global lifting operators in (2.1), (2.2), and (2.3), we obtain

$$\begin{aligned}
& \sum_{K \in \Omega_h} \left( - \int_K \boldsymbol{\sigma}_h \cdot \nabla v_h \, d\mathbf{x} + \int_{\partial K} v_h \widehat{\boldsymbol{\sigma}}_h \cdot \mathbf{n}_K \, dS \right) \\
&= - \int_{\Omega} \boldsymbol{\sigma}_h \cdot \nabla_h v_h \, d\mathbf{x} + \int_{\mathcal{F}_h^{\mathcal{I}}} \{\!\{ \boldsymbol{\sigma}_h^F \}\!\}_{1-\alpha_F} \cdot [\![ v_h ]\!]_{\mathbf{N}} \, dS + \int_{\mathcal{F}_h^{\mathcal{D}}} v_h \boldsymbol{\sigma}_h^F \cdot \mathbf{n}_{\Omega} \, dS - \int_{\mathcal{F}_h^{\mathcal{N}}} g_{\mathbf{N}} v_h \, dS \\
&= \int_{\Omega} \boldsymbol{\kappa} (\nabla_h u_h - \mathcal{L}_h u_h) \cdot \nabla_h v_h \, d\mathbf{x} + \sum_{F \in \mathcal{F}_h^{\mathcal{I}}} \int_{\Omega} \boldsymbol{\sigma}_h^F \cdot \mathcal{L}^F ([\![ v_h ]\!]_{\mathbf{N}}) \, d\mathbf{x} \\
&\quad + \sum_{F \in \mathcal{F}_h^{\mathcal{D}}} \int_{\Omega} \boldsymbol{\sigma}_h^F \cdot \mathcal{L}_{\mathcal{D}}^F (v_h|_F) \, d\mathbf{x} - \int_{\mathcal{F}_h^{\mathcal{N}}} g_{\mathbf{N}} v_h \, dS + \int_{\mathcal{F}_h^{\mathcal{D}}} g_{\mathbf{D}} (\boldsymbol{\kappa} \nabla_h v_h \cdot \mathbf{n}_{\Omega}) \, dS \\
&= \int_{\Omega} \boldsymbol{\kappa} (\nabla_h u_h - \mathcal{L}_h u_h) \cdot \nabla_h v_h \, d\mathbf{x} - \sum_{F \in \mathcal{F}_h^{\mathcal{I}}} \int_{\Omega} \boldsymbol{\kappa} (\nabla_h u_h - \chi_F \mathcal{L}^F ([\![ u_h ]\!]_{\mathbf{N}})) \cdot \mathcal{L}^F ([\![ v_h ]\!]_{\mathbf{N}}) \, d\mathbf{x} \\
&\quad - \sum_{F \in \mathcal{F}_h^{\mathcal{D}}} \int_{\Omega} \boldsymbol{\kappa} (\nabla_h u_h - \chi_F \mathcal{L}_{\mathcal{D}}^F (u_h|_F - g_{\mathbf{D}})) \cdot \mathcal{L}_{\mathcal{D}}^F (v_h|_F) \, d\mathbf{x} \\
&\quad - \int_{\mathcal{F}_h^{\mathcal{N}}} g_{\mathbf{N}} v_h \, dS + \int_{\mathcal{F}_h^{\mathcal{D}}} g_{\mathbf{D}} (\boldsymbol{\kappa} \nabla_h v_h \cdot \mathbf{n}_{\Omega}) \, dS \\
&= \int_{\Omega} \boldsymbol{\kappa} (\nabla_h u_h - \mathcal{L}_h u_h) \cdot \nabla_h v_h \, d\mathbf{x} - \int_{\Omega} \boldsymbol{\kappa} \nabla_h u_h \cdot \mathcal{L}_h v_h \, d\mathbf{x} \\
&\quad + \sum_{F \in \mathcal{F}_h^{\mathcal{I}}} \chi_F \int_{\Omega} \boldsymbol{\kappa} \mathcal{L}^F ([\![ u_h ]\!]_{\mathbf{N}}) \cdot \mathcal{L}^F ([\![ v_h ]\!]_{\mathbf{N}}) \, d\mathbf{x} + \sum_{F \in \mathcal{F}_h^{\mathcal{D}}} \chi_F \int_{\Omega} \boldsymbol{\kappa} \mathcal{L}_{\mathcal{D}}^F (u_h|_F) \cdot \mathcal{L}_{\mathcal{D}}^F (v_h|_F) \, d\mathbf{x} \\
&\quad - \int_{\mathcal{F}_h^{\mathcal{N}}} g_{\mathbf{N}} v_h \, dS + \int_{\mathcal{F}_h^{\mathcal{D}}} g_{\mathbf{D}} (\boldsymbol{\kappa} (\nabla_h v_h - \chi_F \mathcal{L}_{\mathcal{D}}^F v_h) \cdot \mathbf{n}_{\Omega}) \, dS.
\end{aligned}$$

Therefore, we get the following reduced formulation in terms of the primal variable only: find  $u_h \in \mathcal{V}_h^p$  such that

$$\mathcal{A}_h(u_h, v_h) = \ell_h(v_h) \quad \forall v_h \in \mathcal{V}_h^p, \quad (2.13)$$

where the bilinear form  $\mathcal{A}_h : \mathcal{V}_h^p \times \mathcal{V}_h^p \rightarrow \mathbb{R}$  and the linear functional  $\ell_h : \mathcal{V}_h^p \rightarrow \mathbb{R}$  are given by

$$\begin{aligned}
\mathcal{A}_h(u_h, v_h) &:= \int_{\Omega} \boldsymbol{\kappa} (\nabla_h u_h - \mathcal{L}_h u_h) \cdot \nabla_h v_h \, d\mathbf{x} - \int_{\Omega} \boldsymbol{\kappa} \nabla_h u_h \cdot \mathcal{L}_h v_h \, d\mathbf{x} \\
&\quad + \sum_{F \in \mathcal{F}_h^{\mathcal{I}}} \chi_F \int_{\Omega} \boldsymbol{\kappa} \mathcal{L}^F ([\![ u_h ]\!]_{\mathbf{N}}) \cdot \mathcal{L}^F ([\![ v_h ]\!]_{\mathbf{N}}) \, d\mathbf{x} + \sum_{F \in \mathcal{F}_h^{\mathcal{D}}} \chi_F \int_{\Omega} \boldsymbol{\kappa} \mathcal{L}_{\mathcal{D}}^F (u_h|_F) \cdot \mathcal{L}_{\mathcal{D}}^F (v_h|_F) \, d\mathbf{x}, \quad (2.14a)
\end{aligned}$$

$$\ell_h(v_h) := \int_{\Omega} f v_h \, d\mathbf{x} + \int_{\mathcal{F}_h^{\mathcal{N}}} g_{\mathbf{N}} v_h \, dS - \int_{\mathcal{F}_h^{\mathcal{D}}} g_{\mathbf{D}} (\boldsymbol{\kappa} (\nabla_h v_h - \chi_F \mathcal{L}_{\mathcal{D}}^F v_h) \cdot \mathbf{n}_{\Omega}) \, dS. \quad (2.14b)$$

## 2.4 Well-posedness

We define the following mesh-dependent seminorm in  $\mathcal{V}_h^p + H^1(\Omega_h)$ :

$$\|v\|_{\text{CDG}}^2 := \|\sqrt{\boldsymbol{\kappa}} \nabla_h v\|_{L^2(\Omega)^d}^2 + \sum_{F \in \mathcal{F}_h^{\mathcal{I}}} \chi_F \|\sqrt{\boldsymbol{\kappa}} \mathcal{L}^F ([\![ v ]\!]_{\mathbf{N}})\|_{L^2(\Omega)^d}^2 + \sum_{F \in \mathcal{F}_h^{\mathcal{D}}} \chi_F \|\sqrt{\boldsymbol{\kappa}} \mathcal{L}_{\mathcal{D}}^F (v|_F)\|_{L^2(\Omega)^d}^2,$$

where  $\sqrt{\boldsymbol{\kappa}}$  is the symmetric positive definite matrix such that  $\sqrt{\boldsymbol{\kappa}} \cdot \sqrt{\boldsymbol{\kappa}} = \boldsymbol{\kappa}$ .

The existence and uniqueness of a discrete solution to (2.13) is a consequence of the following lemmas, where we show that  $\|\cdot\|_{\text{CDG}}$  is a norm in  $\mathcal{V}_h^p$  provided that Assumption 2.1 holds, and that the bilinear form  $\mathcal{A}_h(\cdot, \cdot)$  is coercive with respect to  $\|\cdot\|_{\text{CDG}}$ .

**Lemma 2.7.** *Under Assumption 2.1, the seminorm  $\|\cdot\|_{\text{CDG}}$  is a norm in the discrete space  $\mathcal{V}_h^p$ .*

*Proof.* Let  $v_h \in \mathcal{V}_h^p$  with  $\|v_h\|_{\text{CDG}} = 0$ . Due to the nondegeneracy in (1.1) of  $\boldsymbol{\kappa}$ , we deduce that  $\mathcal{L}^F ([\![ u_h ]\!]_{\mathbf{N}}) = 0$  for all  $F \in \mathcal{F}_h^{\mathcal{I}}$ , and  $\mathcal{L}_{\mathcal{D}}^F (v_h|_F) = 0$  for all  $F \in \mathcal{F}_h^{\mathcal{D}}$ . Moreover, from the definition in (2.1) of  $\mathcal{L}^F(\cdot)$  and Assumption 2.1, for each  $F \in \mathcal{F}_h^{\mathcal{I}}$  shared by two elements  $K_1, K_2 \in \Omega_h$  with  $p_{K_1} > p_{K_2}$ , we get

$$\int_F [\![ v_h ]\!]_{\mathbf{N}} \cdot \{\!\{ \mathbf{r}_h \}\!\}_{1-\alpha_F} \, dS = \int_F [\![ v_h ]\!]_{\mathbf{N}} \cdot \mathbf{r}_h|_{K_1} \, dS = 0 \quad \forall \mathbf{r}_h \in \mathcal{M}_h^p. \quad (2.15)$$

In order to show that  $\llbracket v_h \rrbracket_N = 0$  on  $F$ , it is enough to choose  $\mathbf{r}_h$  in (2.15) as a polynomial whose restriction to  $F$  is equal to  $\llbracket v_h \rrbracket_N$ , is constant along the orthogonal direction to  $F$ , and has support on  $K_1$ . Since  $\llbracket v_h \rrbracket_N$  is a  $d$ -vector-valued polynomial of degree  $\max\{p_{K_1}, p_{K_2}\} = p_{K_1}$  defined on  $F$ , such a choice is only possible because  $\alpha_F$  was chosen in Assumption 2.1 such that  $\{\mathbf{r}_h\}_{1-\alpha_F}$  reduces to the trace of  $\mathbf{r}_h$  from the element of higher degree. The choice of  $\alpha_F$  is not relevant when  $p_{K_1} = p_{K_2}$ ; in that case, we can always show that  $\llbracket v_h \rrbracket_N = 0$ . Using the definition in (2.2) of  $\mathcal{L}_D^F(\cdot)$ , one can prove that  $v_h = 0$  on  $\Gamma_D$ . In addition,  $\nabla_h v_h = 0$  in  $\Omega$ , so we deduce that  $v_h$  is a piecewise constant function on the mesh  $\Omega_h$ . Considering that  $\llbracket v_h \rrbracket_N = 0$ , it follows that  $v_h$  is a constant function on  $\Omega$ , and moreover, it has zero trace on  $\Gamma_D$ . Since  $|\Gamma_D| > 0$ , we conclude that  $v_h = 0$ .  $\square$

**Lemma 2.8** (Coercivity of  $\mathcal{A}_h$ ). *Under Assumptions 2.1 and 2.2, there exists a positive constant  $C_A$  independent of the meshsize  $h$ , the degree vector  $\mathbf{p}$ , and the maximum number of facets of  $\Omega_h$  such that*

$$\mathcal{A}_h(v_h, v_h) \geq C_A \llbracket v_h \rrbracket_{\text{CDG}}^2 \quad \forall v_h \in \mathcal{V}_h^{\mathbf{p}}. \quad (2.16)$$

*Proof.* Let  $v_h \in \mathcal{V}_h^{\mathbf{p}}$ . From the definition in (2.14a) of the bilinear form  $\mathcal{A}_h(\cdot, \cdot)$ , and using the symmetry of  $\mathcal{A}_h(\cdot, \cdot)$  and the Young inequality, we obtain

$$\begin{aligned} \mathcal{A}_h(v_h, v_h) &= \|\sqrt{\kappa} \nabla_h v_h\|_{L^2(\Omega)^d}^2 - 2 \int_{\Omega} \kappa \mathcal{L}_h v_h \cdot \nabla_h v_h \, d\mathbf{x} + \sum_{F \in \mathcal{F}_h^{\mathcal{I}}} \chi_F \|\sqrt{\kappa} \mathcal{L}^F(\llbracket v_h \rrbracket_N)\|_{L^2(\Omega)^d}^2 \\ &\quad + \sum_{F \in \mathcal{F}_h^{\mathcal{D}}} \chi_F \|\sqrt{\kappa} \mathcal{L}_D^F(v_h|_F)\|_{L^2(\Omega)^d}^2 \\ &\geq (1 - \varepsilon) \|\sqrt{\kappa} \nabla_h v_h\|_{L^2(\Omega)^d}^2 - \frac{1}{\varepsilon} \|\sqrt{\kappa} \mathcal{L}_h v_h\|_{L^2(\Omega)^d}^2 + \sum_{F \in \mathcal{F}_h^{\mathcal{I}}} \chi_F \|\sqrt{\kappa} \mathcal{L}^F(\llbracket v_h \rrbracket_N)\|_{L^2(\Omega)^d}^2 \\ &\quad + \sum_{F \in \mathcal{F}_h^{\mathcal{D}}} \chi_F \|\sqrt{\kappa} \mathcal{L}_D^F(v_h|_F)\|_{L^2(\Omega)^d}^2. \end{aligned} \quad (2.17)$$

It only remains to bound the second term on the right-hand side of (2.17). Using the definition of the global lifting  $\mathcal{L}_h v_h$ , the definition in (2.6) of the set  $\mathcal{F}_K^{\text{out}}$ , and the standard inequality  $|\mathbf{y}|_1 \leq \sqrt{n} |\mathbf{y}|_2$  for vectors in  $\mathbb{R}^n$ , we get

$$\begin{aligned} \|\sqrt{\kappa} \mathcal{L}_h v_h\|_{L^2(\Omega)^d}^2 &= \sum_{K \in \Omega_h} \int_K \left( \sum_{F \in \mathcal{F}_K^{\text{out}} \cap \mathcal{F}_h^{\mathcal{I}}} \sqrt{\kappa} \mathcal{L}^F(\llbracket v_h \rrbracket_N) + \sum_{F \in \mathcal{F}_K^{\text{out}} \cap \mathcal{F}_h^{\mathcal{D}}} \sqrt{\kappa} \mathcal{L}_D^F(v_h|_F) \right)^2 \, d\mathbf{x} \\ &\leq \sum_{K \in \Omega_h} \nu_F^{\text{out}} \left( \sum_{F \in \mathcal{F}_K^{\text{out}} \cap \mathcal{F}_h^{\mathcal{I}}} \|\sqrt{\kappa} \mathcal{L}^F(\llbracket v_h \rrbracket_N)\|_{L^2(K)^d}^2 + \sum_{F \in \mathcal{F}_K^{\text{out}} \cap \mathcal{F}_h^{\mathcal{D}}} \|\sqrt{\kappa} \mathcal{L}_D^F(v_h|_F)\|_{L^2(K)^d}^2 \right) \\ &= \sum_{F \in \mathcal{F}_h^{\mathcal{I}}} \nu_F^{\text{out}} \|\sqrt{\kappa} \mathcal{L}^F(\llbracket v_h \rrbracket_N)\|_{L^2(\Omega)^d}^2 + \sum_{F \in \mathcal{F}_h^{\mathcal{D}}} \nu_F^{\text{out}} \|\sqrt{\kappa} \mathcal{L}_D^F(v_h|_F)\|_{L^2(\Omega)^d}^2. \end{aligned} \quad (2.18)$$

Combining (2.18) with (2.17), and using Assumption 2.2, it follows that

$$\begin{aligned} \mathcal{A}_h(v_h, v_h) &\geq (1 - \varepsilon) \|\sqrt{\kappa} \nabla_h v_h\|_{L^2(\Omega)^d}^2 + \sum_{F \in \mathcal{F}_h^{\mathcal{I}}} \left( \chi_F - \frac{\nu_F^{\text{out}}}{\varepsilon} \right) \|\sqrt{\kappa} \mathcal{L}^F(\llbracket v_h \rrbracket_N)\|_{L^2(\Omega)^d}^2 \\ &\quad + \sum_{F \in \mathcal{F}_h^{\mathcal{D}}} \left( \chi_F - \frac{\nu_F^{\text{out}}}{\varepsilon} \right) \|\sqrt{\kappa} \mathcal{L}_D^F(v_h|_F)\|_{L^2(\Omega)^d}^2 \\ &\geq (1 - \varepsilon) \|\sqrt{\kappa} \nabla_h v_h\|_{L^2(\Omega)^d}^2 + \sum_{F \in \mathcal{F}_h^{\mathcal{I}}} \chi_F \left( 1 - \frac{\gamma}{\varepsilon} \right) \|\sqrt{\kappa} \mathcal{L}^F(\llbracket v_h \rrbracket_N)\|_{L^2(\Omega)^d}^2 \\ &\quad + \sum_{F \in \mathcal{F}_h^{\mathcal{D}}} \chi_F \left( 1 - \frac{\gamma}{\varepsilon} \right) \|\sqrt{\kappa} \mathcal{L}_D^F(v_h|_F)\|_{L^2(\Omega)^d}^2. \end{aligned}$$

Therefore, since  $0 < \gamma < 1$ , we can choose  $\gamma < \varepsilon < 1$ . This completes the proof of (2.16).  $\square$

In the error analysis of next section, we use the following continuity property of the bilinear form  $\mathcal{A}_h(\cdot, \cdot)$ , which can be easily obtained using the Cauchy–Schwarz inequality and bound (2.18) on  $\mathcal{L}_h v_h$ .

**Lemma 2.9** (Continuity of  $\mathcal{A}_h(\cdot, \cdot)$ ). *Under Assumption 2.1, it holds*

$$\mathcal{A}_h(u, v) \leq 2 \llbracket u \rrbracket_{\text{CDG}} \llbracket v \rrbracket_{\text{CDG}} \quad \forall u, v \in H^1(\Omega_h).$$

### 3 Convergence analysis

In this section, we derive *hp-a priori* error estimates for the CDG method. Henceforth, we denote by  $\mathbf{I}$  the identity operator for  $d$ -vector-valued functions, and we use  $a \lesssim b$  to indicate the existence of a positive constant  $C$  independent of  $h$ ,  $\mathbf{p}$ , and the maximum number of facets of the elements in  $\Omega_h$  such that  $a \leq Cb$ . Similarly, we use  $a \simeq b$  whenever  $a \lesssim b$  and  $b \lesssim a$ .

The second Strang's lemma and the coercivity and continuity in Lemmas 2.8 and 2.9 of the bilinear form  $\mathcal{A}_h(\cdot, \cdot)$  lead to the following *a priori* error bound.

**Lemma 3.1** (*A priori* error bound). *Let Assumptions 2.1 and 2.2 hold. Let also the diffusion coefficient  $\boldsymbol{\kappa}$  and the continuous weak solution  $u$  to (1.2) satisfy:  $u \in H_{\Gamma_D}^1(\Omega)$  and  $-\nabla \cdot (\boldsymbol{\kappa} \nabla u) \in L^2(\Omega)$ , and let  $u_h \in \mathcal{V}_h^{\mathbf{p}}$  be the solution to the discrete formulation (2.13). Then, the following error bound holds:*

$$\|u - u_h\|_{\text{CDG}} \leq \left(1 + \frac{2}{C_A}\right) \|u - w_h\|_{\text{CDG}} + \frac{1}{C_A} \sup_{v_h \in \mathcal{V}_h^{\mathbf{p}} \setminus \{0\}} \frac{|\mathcal{A}_h(u, v_h) - \ell_h(v_h)|}{\|v_h\|_{\text{CDG}}},$$

for all  $w_h \in \mathcal{V}_h^{\mathbf{p}}$ .

So far, we have made no assumptions on the family of polytopal meshes  $\{\Omega_h\}_{h>0}$ . In fact, as for the LDG method (see [16, Prop. 2.1]), the well-posedness of (2.13) does not rely on any of such assumptions. However, in the convergence analysis, we require the following assumption (cf. [12, Asm. 30 in Ch. 4.3]).

**Assumption 3.2** (Mesh assumption). *For any  $K \in \Omega_h$ , there exists a set of nonoverlapping  $d$ -dimensional simplices  $\{s_K^F\}_{F \in \mathcal{F}_K}$  such that, for all  $F \in \mathcal{F}_K$ ,  $s_K^F \subset K$  and shares the facet  $F$  with  $K$ , and the following condition holds:*

$$h_K \leq C_s \frac{d|s_K^F|}{|F|},$$

where  $C_s$  is a positive constant independent of the discretization parameters, the measure of  $F$ , and the maximum number of facets of  $K$ .

We further recall the notion of *covering* of a polytopal mesh, as well as the concept of *covering choice function* introduced in [22, Def. 2.2].

**Definition 3.3** (Covering of  $\Omega_h$ ). *For each  $\Omega_h$ , we call a covering  $\mathcal{T}^\#$  of  $\Omega_h$  a set of simplices or hypercubes such that, for each  $K \in \Omega_h$ , there is at least one  $\mathcal{K} \in \mathcal{T}^\#$  with  $K \subset \mathcal{K}$ . We say that  $\varphi : \Omega_h \rightarrow \mathcal{T}^\#$  is a covering choice function if  $K \subset \varphi(K)$  for all  $K \in \Omega_h$ .*

#### 3.1 Some useful tools

The following trace inequalities for discrete (see [33, Thm. 3]) and continuous (see [19, Eq. (1.52) in Ch. 1]) functions are instrumental in the *a priori* error analysis.

**Lemma 3.4** (Trace inequalities). *Let Assumption 3.2 on  $\Omega_h$  hold. Then, for all  $F \in \mathcal{F}_h^{\mathcal{I}} \cup \mathcal{F}_h^{\mathcal{D}}$ , there hold*

$$\|v_h\|_{L^2(F)}^2 \leq \frac{(p_{K_F} + 1)(p_{K_F} + d)}{d} \frac{|F|}{|s_K^F|} \|v_h\|_{L^2(s_K^F)}^2 \quad \forall v_h \in \mathcal{P}^{p_K}(K_F), \quad (3.1a)$$

$$\|v\|_{L^2(F)}^2 \leq C_{\text{tr}} \left( \frac{p_{K_F}}{h_{K_F}} \|v\|_{L^2(s_K^F)}^2 + \frac{h_{K_F}}{p_{K_F}} |v|_{H^1(s_K^F)}^2 \right) \quad \forall v \in H^1(K_F), \quad (3.1b)$$

where  $K_F$  is as in (2.8), and  $s_K^F$  is as in Assumption 3.2.

In order to get a suitable bound on the inconsistency term in Lemma 3.1, we first extend the result in [10, Lemma 2] to polytopal meshes, where Assumption 2.1 on the choice of the weighted-average parameters  $\alpha_F$  plays a crucial role.

**Lemma 3.5** (Jump-lifting bounds). *Under Assumptions 2.1 and 3.2, for all  $v \in H^1(\Omega_h)$ ,  $\mathbf{v} \in H^1(\Omega_h)^d$ , and  $v_h \in \mathbf{M}_h^p$ , there hold*

$$\|[\![v_h]\!]_{\mathbf{N}}\|_{L^2(F)^d} \leq h_{K_F}^{1/2} \|\mathcal{L}^F([\![v_h]\!]_{\mathbf{N}})\|_{L^2(\Omega)^d} \quad \forall F \in \mathcal{F}_h^{\mathcal{T}}, \quad (3.2a)$$

$$\|v_h\|_{L^2(F)} \leq h_{K_F}^{1/2} \|\mathcal{L}_{\mathcal{D}}^F(v_h|_F)\|_{L^2(\Omega)^d} \quad \forall F \in \mathcal{F}_h^{\mathcal{D}}, \quad (3.2b)$$

$$\|\mathcal{L}^F([\![\mathbf{v}]\!]_{\mathbf{N}})\|_{L^2(\Omega)^d} \leq \sqrt{C_s \frac{(p_{K_F}+1)(p_{K_F}+d)}{h_{K_F}}} \|[\![\mathbf{v}]\!]_{\mathbf{N}}\|_{L^2(F)^d} \quad \forall F \in \mathcal{F}_h^{\mathcal{T}}, \quad (3.2c)$$

$$\|\mathcal{L}_{\mathcal{D}}^F(v|_F)\|_{L^2(\Omega)^d} \leq \sqrt{C_s \frac{(p_{K_F}+1)(p_{K_F}+d)}{h_{K_F}}} \|v\|_{L^2(F)} \quad \forall F \in \mathcal{F}_h^{\mathcal{T}}, \quad (3.2d)$$

with  $K_F \in \Omega_h$  defined just above (2.8).

*Proof.* For any  $F \in \mathcal{F}_h^{\mathcal{T}}$ , let  $\mathbf{r}_h = \mathbf{r}_h([\![v_h]\!]_{\mathbf{N}}) \in \mathbf{M}_h^p$  be chosen as in the proof of Lemma 2.7 such that  $\{\![\mathbf{r}_h]\!}_{1-\alpha_F} = [\![v_h]\!]_{\mathbf{N}}$  on  $F$ . Then, using the Cauchy–Schwarz inequality and the definition in (2.1) of the local lifting operator, we have

$$\begin{aligned} \|[\![v_h]\!]_{\mathbf{N}}\|_{L^2(F)^d}^2 &= \int_F [\![v_h]\!]_{\mathbf{N}} \cdot [\![v_h]\!]_{\mathbf{N}} \, dS = \int_F [\![v_h]\!]_{\mathbf{N}} \cdot \{\![\mathbf{r}_h([\![v_h]\!]_{\mathbf{N}})]\!}_{1-\alpha_F} \, dS \\ &= \int_{\Omega} \mathcal{L}^F([\![v_h]\!]_{\mathbf{N}}) \cdot \mathbf{r}_h([\![v_h]\!]_{\mathbf{N}}) \, dS \\ &\leq \|\mathcal{L}^F([\![v_h]\!]_{\mathbf{N}})\|_{L^2(\Omega)^d} \|\mathbf{r}_h([\![v_h]\!]_{\mathbf{N}})\|_{L^2(\Omega)^d}. \end{aligned} \quad (3.3)$$

From the definition of  $\mathbf{r}_h([\![v_h]\!]_{\mathbf{N}})$  and Assumption 3.2, we get

$$\|\mathbf{r}_h([\![v_h]\!]_{\mathbf{N}})\|_{L^2(\Omega)^d} \leq h_{K_F}^{1/2} \|[\![v_h]\!]_{\mathbf{N}}\|_{L^2(F)^d},$$

which, combined with (3.3), gives (3.2a). Bound (3.2b) follows analogously.

As for (3.2c), we use the definition in (2.1) of the local lifting operator  $\mathcal{L}^F(\cdot)$ , the Cauchy–Schwarz inequality, the inverse-trace inequality (3.1a), and Assumption 3.2 to obtain

$$\begin{aligned} \|\mathcal{L}^F([\![\mathbf{v}]\!]_{\mathbf{N}})\|_{L^2(\Omega)^d}^2 &= \int_{\Omega} \mathcal{L}^F([\![\mathbf{v}]\!]_{\mathbf{N}}) \cdot \mathcal{L}^F([\![\mathbf{v}]\!]_{\mathbf{N}}) \, dx = \int_F [\![\mathbf{v}]\!]_{\mathbf{N}} \cdot \mathcal{L}^F([\![\mathbf{v}]\!]_{\mathbf{N}})_{|_{K_F}} \, dS \\ &\leq \|[\![\mathbf{v}]\!]_{\mathbf{N}}\|_{L^2(F)^d} \|\mathcal{L}^F([\![\mathbf{v}]\!]_{\mathbf{N}})_{|_{K_F}}\|_{L^2(F)^d} \\ &\leq \sqrt{\frac{(p_{K_F}+1)(p_{K_F}+d)}{d}} \frac{|F|}{|s_K^F|} \|[\![\mathbf{v}]\!]_{\mathbf{N}}\|_{L^2(F)^d} \|\mathcal{L}^F([\![\mathbf{v}]\!]_{\mathbf{N}})\|_{L^2(K_F)^d} \\ &\leq \sqrt{C_s \frac{(p_{K_F}+1)(p_{K_F}+d)}{h_{K_F}}} \|[\![\mathbf{v}]\!]_{\mathbf{N}}\|_{L^2(F)^d} \|\mathcal{L}^F([\![\mathbf{v}]\!]_{\mathbf{N}})\|_{L^2(\Omega)^d}. \end{aligned}$$

The proof of bound (3.2d) is analogous.  $\square$

The last ingredient is the following approximation result from [22, Lemma 2.3], which not only generalizes the corresponding result in [11, Lemma 4.31] to non-Lipschitz domains, but also removes the usual assumption that the number of mesh elements in  $\Omega_h$  that can intersect each covering element in  $\mathcal{T}^{\#}$  is uniformly bounded.

**Lemma 3.6** (Estimates for  $\tilde{\Pi}_{hp}$ ). *Let Assumption 3.2 on  $\{\Omega_h\}_{h>0}$  hold, and assume that  $h \lesssim 1$ . Let also  $\mathcal{T}^{\#}$  and  $\varphi : \Omega_h \rightarrow \mathcal{T}^{\#}$  be a shape-regular covering of  $\Omega_h$  and a covering choice function, respectively. Suppose that  $u \in L^2(\Omega)$  and that there exist  $l_{\mathcal{K}} \geq 0$  and  $\mathcal{U}_{\mathcal{K}} \in H^{l_{\mathcal{K}}}(\mathcal{K})$  such that  $(\mathcal{U}_{\mathcal{K}})_{|_{K}} = u|_K$  for each  $K \in \varphi^{-1}(\mathcal{K})$ . Then, for each  $\mathcal{K} \in \mathcal{T}^{\#}$ , there exists an operator  $\tilde{\Pi}_{hp}^{\mathcal{K}} : H^{l_{\mathcal{K}}}(\mathcal{K}) \rightarrow \mathcal{P}^{p_{\mathcal{K}}}(\mathcal{K})$  such that*

$$\left( \sum_{K \in \varphi^{-1}(\mathcal{K})} \|u - \tilde{\Pi}_{hp}^{\mathcal{K}} u\|_{H^q(K)}^2 \right)^{1/2} \lesssim \frac{h_{\mathcal{K}}^{\ell_{\mathcal{K}}-q}}{p_{\mathcal{K}}^{l_{\mathcal{K}}-q}} \|\mathcal{U}_{\mathcal{K}}\|_{H^{l_{\mathcal{K}}}(\mathcal{K})}, \quad \text{for } 0 \leq q \leq l_{\mathcal{K}},$$

where  $h_{\mathcal{K}} := \text{diam}(\mathcal{K})$ ,  $p_{\mathcal{K}} := \min_{K \in \varphi^{-1}(\mathcal{K})} p_K$ ,  $\ell_{\mathcal{K}} := \min\{p_{\mathcal{K}}+1, l_{\mathcal{K}}\}$ , and the hidden constant depends only on  $d$ ,  $l_{\mathcal{K}}$ , and the shape-regularity constant of  $\mathcal{T}^{\#}$ .

A typical choice for the extension operator in the statement of Lemma 3.6 is the one proposed by Stein in [31, Thm. 5 in Ch. VI].

### 3.2 *A priori* error estimates

In next lemma, we get a bound on the inconsistency term in Lemma 3.1. Since we do not have a stability term in the method (see (2.13)), the jump terms must be controlled by the local lifting functions using Lemma 3.5.

**Lemma 3.7** (Bound on the inconsistency term). *Let the assumptions of Lemma 3.1 hold. Then,*

$$\begin{aligned} \sup_{v_h \in \mathcal{V}_h^p \setminus \{0\}} \frac{|\mathcal{A}_h(u, v_h) - \ell_h(v_h)|}{\|v_h\|_{\text{CDG}}} &\leq \frac{1}{\sqrt{k_\star}} \left( \sum_{F \in \mathcal{F}_h^\mathcal{I}} \frac{h_{K_F}}{\chi_F} \|\{(\mathbf{I} - \boldsymbol{\Pi}_h)(\boldsymbol{\kappa} \nabla u)\}_{1-\alpha_F}\|_{L^2(F)^d}^2 \right. \\ &\quad \left. + \sum_{F \in \mathcal{F}_h^\mathcal{D}} \frac{h_{K_F}}{\chi_F} \|(\mathbf{I} - \boldsymbol{\Pi}_h)(\boldsymbol{\kappa} \nabla u) \cdot \mathbf{n}_\Omega\|_{L^2(F)}^2 \right)^{1/2}. \end{aligned} \quad (3.4)$$

*Proof.* For all  $v_h \in \mathcal{V}_h^p$ , integration by parts and standard arguments lead to the following identity:

$$\mathcal{A}_h(u, v_h) - \ell_h(v_h) = \int_{\mathcal{F}_h^\mathcal{I}} \{(\mathbf{I} - \boldsymbol{\Pi}_h)(\boldsymbol{\kappa} \nabla u)\}_{1-\alpha_F} \cdot [v_h]_{\mathbf{N}} \, dS + \int_{\mathcal{F}_h^\mathcal{D}} v_h (\mathbf{I} - \boldsymbol{\Pi}_h)(\boldsymbol{\kappa} \nabla u) \cdot \mathbf{n}_\Omega \, dS,$$

which, together with the Cauchy–Schwarz inequality and bounds (3.2a) and (3.2b), implies (3.4).  $\square$

The following local quasi-uniformity conditions are used to simplify some terms in the *a priori* error estimate in Theorem 3.9.

**Assumption 3.8** (Local quasi-uniformity). *We assume that  $\{\Omega_h\}_{h>0}$  and the degree vectors  $\mathbf{p} = (p_K)_{K \in \Omega_h}$  satisfy the following local quasi-uniformity conditions: for all neighboring elements  $K, K' \in \Omega_h$*

$$h_K \simeq h_{K'} \quad \text{and} \quad p_K \simeq p_{K'}.$$

Moreover, for all  $\mathcal{K} \in \mathcal{T}^\#$ , we assume that

$$h_{\mathcal{K}} \lesssim h_K \quad \text{and} \quad p_K \lesssim p_{\mathcal{K}} \quad \text{for all } K \in \varphi^{-1}(\mathcal{K}).$$

**Theorem 3.9** (*A priori* error estimates). *Let the assumptions of Lemma 3.1 and Assumption 3.8 hold, and assume that  $\{\Omega_h\}_{h>0}$  and the continuous weak solution  $u$  to (1.2) satisfy the assumptions of Lemma 3.6 with  $l_{\mathcal{K}} > 3/2$ . Then, for a sufficiently smooth diffusion coefficient  $\boldsymbol{\kappa}$ , we have*

$$\begin{aligned} \|u - u_h\|_{\text{CDG}}^2 &\lesssim \sum_{\mathcal{K} \in \mathcal{T}^\#} \left( p_{\mathcal{K}}^{-1} + \max_{K \in \varphi^{-1}(\mathcal{K})} \left( \max_{F \in \mathcal{F}_K^\diamond} \chi_F \right) \right) \frac{h_{\mathcal{K}}^{2\ell_{\mathcal{K}}-2}}{p_{\mathcal{K}}^{2l_{\mathcal{K}}-3}} \|\mathcal{U}_{\mathcal{K}}\|_{H^{l_{\mathcal{K}}}(\mathcal{K})}^2 \\ &\quad \sum_{\mathcal{K} \in \mathcal{T}^\#} \max_{K \in \varphi^{-1}(\mathcal{K})} \left( \max_{F \in \mathcal{F}_K^\diamond} \chi_F^{-1} \right) (1 + p_{\mathcal{K}}) \frac{h_{\mathcal{K}}^{2\ell_{\mathcal{K}}-2}}{p_{\mathcal{K}}^{2l_{\mathcal{K}}-3}} \|\boldsymbol{\kappa} \nabla \mathcal{U}_{\mathcal{K}}\|_{H^{l_{\mathcal{K}}-1}(\mathcal{K})^d}^2, \end{aligned} \quad (3.5)$$

where  $\ell_{\mathcal{K}} = \min\{p_{\mathcal{K}} + 1, l_{\mathcal{K}}\}$  and  $\mathcal{F}_K^\diamond := \mathcal{F}_K \cap (\mathcal{F}_h^\mathcal{I} \cup \mathcal{F}_h^\mathcal{D})$ .

*Proof.* Combining the *a priori* error bound in Lemma 3.1 with the bound on the inconsistency term in Lemma 3.7, and choosing  $w_h \in \mathcal{V}_h^p$  as

$$w_{h|_K} := (\tilde{\Pi}_{hp}^{\varphi(K)} u)|_K \quad \forall K \in \Omega_h,$$

we get

$$\begin{aligned} \|u - u_h\|_{\text{CDG}}^2 &\lesssim \|\sqrt{\boldsymbol{\kappa}} \nabla_h(u - \tilde{\Pi}_{hp} u)\|_{L^2(\Omega)^d}^2 + \sum_{F \in \mathcal{F}_h^\mathcal{I}} \chi_F \|\sqrt{\boldsymbol{\kappa}} \mathcal{L}^F([u - \tilde{\Pi}_{hp} u]_{\mathbf{N}})\|_{L^2(\Omega)^d}^2 \\ &\quad + \sum_{F \in \mathcal{F}_h^\mathcal{D}} \chi_F \|\sqrt{\boldsymbol{\kappa}} \mathcal{L}_D^F(u|_F - (\tilde{\Pi}_{hp} u)|_F)\|_{L^2(\Omega)^d}^2 + \sum_{F \in \mathcal{F}_h^\mathcal{I} \cup \mathcal{F}_h^\mathcal{D}} \frac{h_{K_F}}{k_\star \chi_F} \|(\mathbf{I} - \boldsymbol{\Pi}_h)(\boldsymbol{\kappa} \nabla u)|_{K_F}\|_{L^2(F)^d}^2 \\ &=: J_1 + J_2 + J_3 + J_4. \end{aligned} \quad (3.6)$$

In (3.6) and what follows, we omit the explicit dependence of the projection operator  $\tilde{\Pi}_{hp}$  on  $\varphi(K)$  for the sake of simplicity.

We now estimate the terms  $\{J_i\}_{i=1}^4$ . Since  $\kappa \in L^\infty(\Omega)^{d \times d}$ , by using the approximation properties in Lemma 3.6 of  $\tilde{\Pi}_{hp}$ , we have

$$J_1 = \sum_{K \in \Omega_h} \|\sqrt{\kappa} \nabla (u - \tilde{\Pi}_{hp} u)\|_{L^2(K)}^2 \lesssim \sum_{\mathcal{K} \in \mathcal{T}^\#} \frac{h_{\mathcal{K}}^{2\ell_{\mathcal{K}}-2}}{p_{\mathcal{K}}^{2l_{\mathcal{K}}-2}} \|\mathcal{U}_{\mathcal{K}}\|_{H^{l_{\mathcal{K}}}(\mathcal{K})}^2. \quad (3.7)$$

For each  $K \in \Omega_h$ , let  $\mathcal{F}_K^\diamond := \mathcal{F}_K \cap (\mathcal{F}_h^\mathcal{I} \cup \mathcal{F}_h^\mathcal{D})$ . Using bounds (3.2c) and (3.2d), the trace inequality (3.1b), the approximation properties in Lemma 3.6 of  $\tilde{\Pi}_{hp}$ , and Assumption 3.8, we obtain

$$\begin{aligned} J_2 + J_3 &= \sum_{F \in \mathcal{F}_h^\mathcal{I}} \chi_F \|\sqrt{\kappa} \mathcal{L}^F ([u - \tilde{\Pi}_{hp} u]_{\mathbb{N}})\|_{L^2(\Omega)^d}^2 + \sum_{F \in \mathcal{F}_h^\mathcal{D}} \chi_F \|\sqrt{\kappa} \mathcal{L}_{\mathcal{D}}^F (u|_F - (\tilde{\Pi}_{hp} u)|_F)\|_{L^2(\Omega)^d}^2 \\ &\lesssim \sum_{F \in \mathcal{F}_h^\mathcal{I}} \frac{\chi_F (p_{K_F} + 1)(p_{K_F} + d)}{h_{K_F}} \| [u - \tilde{\Pi}_{hp} u]_{\mathbb{N}} \|_{L^2(F)^d}^2 \\ &\quad + \sum_{F \in \mathcal{F}_h^\mathcal{D}} \frac{\chi_F (p_{K_F} + 1)(p_{K_F} + d)}{h_{K_F}} \| u|_F - (\tilde{\Pi}_{hp} u)|_F \|_{L^2(F)}^2 \\ &\lesssim \sum_{K \in \Omega_h} \sum_{F \in \mathcal{F}_K^\diamond} \frac{\chi_F (p_{K_F} + 1)(p_{K_F} + d)}{h_{K_F}} \left( \frac{p_K}{h_K} \|u - \tilde{\Pi}_{hp} u\|_{L^2(s_K^F)}^2 + \frac{h_K}{p_K} |u - \tilde{\Pi}_{hp} u|_{H^1(s_K^F)}^2 \right) \\ &\lesssim \sum_{K \in \Omega_h} \left( \max_{F \in \mathcal{F}_K^\diamond} \chi_F \right) \left( \frac{p_K^3}{h_K^2} \|u - \tilde{\Pi}_{hp} u\|_{L^2(K)}^2 + p_K |u - \tilde{\Pi}_{hp} u|_{H^1(K)}^2 \right) \\ &\lesssim \sum_{\mathcal{K} \in \mathcal{T}^\#} \max_{K \in \phi^{-1}(\mathcal{K})} \left( \max_{F \in \mathcal{F}_K^\diamond} \chi_F \right) \frac{h_{\mathcal{K}}^{2\ell_{\mathcal{K}}-2}}{p_{\mathcal{K}}^{2l_{\mathcal{K}}-3}} \|\mathcal{U}_{\mathcal{K}}\|_{H^{l_{\mathcal{K}}}(\mathcal{K})}^2. \end{aligned} \quad (3.8)$$

We denote by  $\tilde{\Pi}_{hp}$  the natural extension of the operator  $\tilde{\Pi}_{hp}$  to  $d$ -vector-valued functions. To estimate the terms  $J_4$  and  $J_5$ , which arise from the inconsistency of the method, we use the triangle inequality, the trace inequalities (3.1a) and (3.1b), the stability of  $\Pi_h$  in the  $L^2(K)$  norm, the approximation properties of  $\tilde{\Pi}_{hp}$ , and Assumption 3.8, as follows:

$$\begin{aligned} J_4 &= \frac{1}{k_\star} \sum_{F \in \mathcal{F}_h^\mathcal{I} \cup \mathcal{F}_h^\mathcal{D}} \frac{h_{K_F}}{\chi_F} \|(\mathbf{I} - \Pi_h)(\kappa \nabla u)|_{K_F}\|_{L^2(F)^d}^2 \\ &\lesssim \sum_{F \in \mathcal{F}_h^\mathcal{I} \cup \mathcal{F}_h^\mathcal{D}} \frac{h_{K_F}}{\chi_F} \left( \|(\mathbf{I} - \tilde{\Pi}_{hp})(\kappa \nabla u)|_{K_F}\|_{L^2(F)^d}^2 + \|\Pi_h(\mathbf{I} - \tilde{\Pi}_{hp})(\kappa \nabla u)|_{K_F}\|_{L^2(F)^d}^2 \right) \\ &\lesssim \sum_{F \in \mathcal{F}_h^\mathcal{I} \cup \mathcal{F}_h^\mathcal{D}} \frac{h_{K_F}}{\chi_F} \left( \frac{p_{K_F}}{h_{K_F}} \|(\mathbf{I} - \tilde{\Pi}_{hp})(\kappa \nabla u)\|_{L^2(s_K^F)^d}^2 + \frac{h_{K_F}}{p_{K_F}} |(\mathbf{I} - \tilde{\Pi}_{hp})(\kappa \nabla u)|_{H^1(s_K^F)^d}^2 \right. \\ &\quad \left. + \frac{C_s(p_{K_F} + 1)(p_{K_F} + d)}{h_{K_F}} \|\Pi_h(\mathbf{I} - \tilde{\Pi}_{hp})(\kappa \nabla u)\|_{L^2(s_K^F)^d}^2 \right) \\ &\lesssim \sum_{K \in \Omega_h} \left( \max_{F \in \mathcal{F}_K^\diamond} \chi_F^{-1} \right) \left[ (p_K + p_K^2) \|(\mathbf{I} - \tilde{\Pi}_{hp})(\kappa \nabla u)\|_{L^2(K)^d}^2 + \frac{h_K^2}{p_K} |(\mathbf{I} - \tilde{\Pi}_{hp})(\kappa \nabla u)|_{H^1(K)^d}^2 \right] \\ &\lesssim \sum_{\mathcal{K} \in \mathcal{T}^\#} \max_{K \in \phi^{-1}(\mathcal{K})} \left( \max_{F \in \mathcal{F}_K^\diamond} \chi_F^{-1} \right) (1 + p_{\mathcal{K}}) \frac{h_{\mathcal{K}}^{2\ell_{\mathcal{K}}-2}}{p_{\mathcal{K}}^{2l_{\mathcal{K}}-3}} \|\kappa \nabla \mathcal{U}_{\mathcal{K}}\|_{H^{l_{\mathcal{K}}-1}(\mathcal{K})^d}^2. \end{aligned} \quad (3.9)$$

Combining (3.7), (3.8), and (3.9) with (3.6), we get (3.5).  $\square$

**Remark 3.10** (Additional suboptimality in  $p_{\mathcal{K}}$ ). *The factor  $(1 + p_{\mathcal{K}})$  in the last term of (3.5) leads to a suboptimality in  $p_{\mathcal{K}}$  that is a power higher than the one typically obtained for most DG methods. This occurs because the simple choice of the extension polynomials used in the proof of the bounds (3.2a) and (3.2b) does not yield the  $p_{\mathcal{K}}^{-1}$  factor obtained for tensor-product meshes (see [29, Lemma 7.1] and [26, Prop. 3]). Recovering the factor  $p_{\mathcal{K}}^{-1}$  for general polytopal meshes is challenging and requires designing a suitable extension polynomial operator.*

*A simple way to avoid such suboptimality is to add, in (2.13), the same stability term used in the LDG method. However, this would over-stabilize the scheme; in fact, the terms in (2.13) involving the local lifting functions already act as a stabilization mechanism in the CDG method (see Remark 2.6). ■*

## 4 Computational aspects

In this section, we present fast algorithms to assemble the linear system  $\mathcal{A} = \mathbf{b}$  for the CDG, the LDG, and the BR2 methods. In particular, these algorithms show that the assembling of the stiffness matrices can be carried out without storing large block-structured matrices. The ideas here are inspired by the analogous algorithm introduced in [17] for the LDG method on simplicial meshes.

Let  $\{K_r\}_{r=1}^{\mathcal{N}_h^{\text{ele}}}$  be a prescribed order of the elements of the polytopal mesh  $\Omega_h$  with total number of elements  $\mathcal{N}_h^{\text{ele}}$ . For  $r = 1, \dots, \mathcal{N}_h^{\text{ele}}$ , we set  $\Lambda_{K_r} := \dim(\mathcal{P}^{p_{K_r}}(K_r))$ , and fix bases  $\Phi_r := \{\phi_i^r\}_{i=1}^{\Lambda_{K_r}}$  and  $\Psi_r := \{\psi_i^r\}_{i=1}^{d \cdot \Lambda_{K_r}}$  of  $\mathcal{P}^{p_{K_r}}(K_r)$  and  $\mathcal{P}^{p_{K_r}}(K_r)^d$ , respectively. Moreover, to avoid unnecessary computations, we set  $\Psi_r = [\Phi_r]^d$ . Fixed bases for the global spaces  $\mathcal{V}_h^p$  and  $\mathcal{M}_h^p$  can then be naturally defined. The implemented code is based on the `lymph` library and the bases are constructed from the tensor product of the Legendre polynomials in one dimension, considering only the 2D polynomials of degree less than or equal to  $p_{K_r}$ . The computation of the integrals is based on a quadrature-free approach for the matrices and on a sub-tessellation of the polygons coupled with Gauss-Legendre rules for the forcing term and the face integrals (see [1, §4.2]).

Let  $\mathbf{M}$ ,  $\mathbf{D}$ ,  $\mathbf{B}^\nabla$ , and  $\mathbf{B}^{\text{av}}$  be the matrices associated with the following bilinear forms:

$$\begin{aligned} \mathbf{m}_h(\mathbf{q}_h, \mathbf{r}_h) &:= \sum_{K \in \Omega_h} \int_K \mathbf{q}_h \cdot \mathbf{r}_h \, dx & \forall (\mathbf{q}_h, \mathbf{r}_h) \in \mathcal{M}_h^p \times \mathcal{M}_h^p, \\ \mathbf{d}_h(\mathbf{q}_h, \mathbf{s}_h) &:= \sum_{K \in \Omega_h} \int_K \kappa \mathbf{q}_h \cdot \mathbf{s}_h \, dx & \forall (\mathbf{q}_h, \mathbf{s}_h) \in \mathcal{M}_h^p \times \mathcal{M}_h^p, \\ \mathbf{b}_h^\nabla(u_h, \mathbf{r}_h) &:= - \sum_{K \in \Omega_h} \int_K \nabla u_h \cdot \mathbf{r}_h \, dx & \forall (u_h, \mathbf{r}_h) \in \mathcal{V}_h^p \times \mathcal{M}_h^p, \\ \mathbf{b}_h^{\text{av}}(u_h, \mathbf{r}_h) &:= \int_{\mathcal{F}_h^{\mathcal{I}}} [\![u_h]\!]_{\mathbf{N}} \cdot \{\!\{ \mathbf{r}_h \}\!\}_{1-\alpha_F} \, dS + \int_{\mathcal{F}_h^{\mathcal{D}}} u_h \mathbf{r}_h \cdot \mathbf{n}_\Omega \, dS & \forall (u_h, \mathbf{r}_h) \in \mathcal{V}_h^p \times \mathcal{M}_h^p. \end{aligned}$$

By definition, the matrices  $\mathbf{M}$ ,  $\mathbf{D}$ , and  $\mathbf{B}^\nabla$  have a block-diagonal structure and their  $r$ th diagonal blocks, which involve only volume integrals, are given by

$$\mathbf{M}_{rr} := \left[ \int_{K_r} \psi_i^r \cdot \psi_j^r \, dx \right]_{ij}, \quad \mathbf{D}_{rr} := \left[ \int_{K_r} \psi_i^r \cdot \kappa_{|K_r} \psi_j^r \, dx \right]_{ij}, \quad \mathbf{B}_{rr}^\nabla := - \left[ \int_{K_r} \psi_i^r \cdot \nabla \phi_j^r \, dx \right]_{ij},$$

where the ranges of the indices  $i$  and  $j$  have been omitted for the sake of simplicity.

The matrix  $\mathbf{B}^{\text{av}}$  has a block structure. In the cases of CDG and weighted LDG (henceforth identified as LDG<sub>W</sub>) methods, a block  $\mathbf{B}_{rs}^{\text{av}}$  is nonzero only if there is a facet  $F \in \mathcal{F}_{K_r}^{\text{out}} \cap \mathcal{F}_{K_s}$  (including the trivial case  $r = s$ ). For each element  $K_r \in \Omega_h$ , let  $\{F_r^{(\ell)}\}_{\ell=1}^{\text{card}(\mathcal{F}_{K_r}^{\text{out}})}$  be the facets in  $\mathcal{F}_{K_r}^{\text{out}}$  with a prescribed order. Each facet  $F_r^{(\ell)}$  adds the following contributions to the diagonal block  $\mathbf{B}_{rr}^{\text{av}}$ , and if  $F_r^{(\ell)} \in \mathcal{F}_h^{\mathcal{I}}$  is shared by  $K_r$  and  $K_{s(\ell)}$ , it also contributes to the off-diagonal block  $\mathbf{B}_{rs(\ell)}^{\text{av}}$  as follows:

$$\mathbf{B}_{rr}^{\text{av}(\ell)} = \left[ \int_{F_r^{(\ell)}} \psi_i^r \cdot (\phi_j^r \mathbf{n}_{K_r}) \, dS \right]_{ij}, \quad \mathbf{B}_{rs(\ell)}^{\text{av}(\ell)} = - \left[ \int_{F_r^{(\ell)}} \psi_i^r \cdot (\phi_j^{s(\ell)} \mathbf{n}_{K_r}) \, dS \right]_{ij}.$$

We now focus on the BR2 and the LDG methods with  $\alpha_F = 1/2$  for all  $f \in \mathcal{F}_h^{\mathcal{I}}$ . This choice of the weighted-average parameters leads to a full stencil for the LDG method (which is therefore identified as LDG<sub>f</sub>). For each element  $K_r \in \Omega_h$ , let  $\{F_r^{(\ell)}\}_{\ell=1}^{\text{card}(\mathcal{F}_{K_r})}$  be the facets in  $\mathcal{F}_{K_r}$  with a prescribed order. Then, the two associated block contributions are

$$\mathbf{B}_{rr}^{\text{av}(\ell)} = \left[ \frac{1}{2} \int_{F_r^{(\ell)}} \psi_i^r \cdot (\phi_j^r \mathbf{n}_{K_r}) \, dS \right]_{ij}, \quad \mathbf{B}_{rs(\ell)}^{\text{av}(\ell)} = - \left[ \frac{1}{2} \int_{F_r^{(\ell)}} \psi_i^r \cdot (\phi_j^{s(\ell)} \mathbf{n}_{K_r}) \, dS \right]_{ij}.$$

In addition, let  $\mathbf{b}_f$  and  $\mathbf{g}$  be the vectors associated with the following linear functionals:

$$\ell(v_h) = \int_{\Omega} f v_h \, dx \quad \forall v_h \in \mathcal{V}_h^p, \quad \text{and} \quad g_h(\mathbf{r}_h) := \int_{\mathcal{F}_h^D} g_D \mathbf{r}_h \cdot \mathbf{n}_\Omega \, dS \quad \forall \mathbf{r}_h \in \mathcal{M}_h^p.$$

The computation of  $\mathbf{b}_f$ , which is the same for all the methods considered, is simple and does not require further details. As for  $\mathbf{g}$ , the following vector contribution is obtained for any  $F_r^{(\ell)} \in \mathcal{F}_h^D \cap \mathcal{F}_{K_r}$ :

$$\mathbf{g}_r^{(\ell)} := \left[ - \int_{F_r^{(\ell)}} \psi_i^r \cdot (g_D \mathbf{n}_{K_r}) \, dS \right]_{ij}.$$

It is then evident that all the local contributions involved in the assembling of the linear systems for these methods are essentially the same, which allows for their implementation in an almost unified framework. In Algorithm 1, we report the procedure to assemble the stiffness matrix  $\mathcal{A}$  and the right-hand side vector  $\mathbf{b}$  for the CDG and BR2 methods. From this algorithm, it can be easily seen that the choice  $\alpha_F = 0$  or  $\alpha_F = 1$  in the CDG method allows us to skip lots of computations, as it reduces the number  $L_r^*$  introduced in line 6 and, consequently, the number of loop iterations in the following lines. In Algorithm 2, we report the corresponding algorithm for both version of the LDG method.

---

**Algorithm 1:** FAST ASSEMBLY OF THE LINEAR SYSTEM FOR THE CDG AND BR2 METHODS

---

```

1 Initialize the matrix  $\mathcal{A}$  and the vector  $\mathbf{b}$ 
2 for  $r = 1$  to  $\mathcal{N}_h^{\text{ele}}$  do
3   Compute  $\mathbf{M}_{rr}^{-1}$ ,  $\mathbf{D}_{rr}$ ,  $\mathbf{B}_{rr}^\nabla$ , and  $\mathbf{b}_{f,r}$ 
4   Set  $\mathbf{D}_{rr} = \mathbf{M}_{rr}^{-1} \mathbf{D}_{rr} \mathbf{M}_{rr}^{-1}$  and  $\mathbf{b}_r = \mathbf{b}_{f,r}$ 
5    $\mathcal{A}_{rr} = \mathcal{A}_{rr} + [\mathbf{B}_{rr}^\nabla]^\top \mathbf{D}_{rr} [\mathbf{B}_{rr}^\nabla]$ 
6   Set  $L_r^* = \text{card}(\mathcal{F}_{K_r}^{\text{out}})$  (for CDG) or  $L_r^* = \text{card}(\mathcal{F}_{K_r})$  (for BR2)
7   for  $\ell = 1$  to  $L_r^*$  do
8     if  $F_r^{(\ell)} \in \mathcal{F}_h^T$  then
9       Set  $s(\ell)$  as the index of the neighbor sharing  $F_r^{(\ell)}$ 
10      Compute the diagonal contribution  $\mathbf{B}_{rr}^{\text{av}(\ell)}$ , the off-diagonal one  $\mathbf{B}_{rs(\ell)}$ , and  $\mathbf{g}_r^{(\ell)}$ 
11       $\mathcal{A}_{rr} = \mathcal{A}_{rr} - [\mathbf{B}_{rr}^\nabla]^\top \mathbf{D}_{rr} [\mathbf{B}_{rr}^{\text{av}(\ell)}] - [\mathbf{B}_{rr}^{\text{av}(\ell)}]^\top \mathbf{D}_{rr} [\mathbf{B}_{rr}^\nabla] + \chi_{F_r^{(\ell)}} [\mathbf{B}_{rr}^{\text{av}(\ell)}]^\top \mathbf{D}_{rr} [\mathbf{B}_{rr}^{\text{av}(\ell)}]$ 
12       $\mathcal{A}_{rs(\ell)} = \mathcal{A}_{rs(\ell)} - [\mathbf{B}_{rr}^\nabla]^\top \mathbf{D}_{rr} [\mathbf{B}_{rs(\ell)}^{\text{av}(\ell)}] + \chi_{F_r^{(\ell)}} [\mathbf{B}_{rr}^{\text{av}(\ell)}]^\top \mathbf{D}_{rr} [\mathbf{B}_{rs(\ell)}^{\text{av}(\ell)}]$ 
13       $\mathcal{A}_{s(\ell)r} = \mathcal{A}_{s(\ell)r} - [\mathbf{B}_{rs(\ell)}^{\text{av}(\ell)}]^\top \mathbf{D}_{rr} [\mathbf{B}_{rr}^\nabla] + \chi_{F_r^{(\ell)}} [\mathbf{B}_{rs(\ell)}^{\text{av}(\ell)}]^\top \mathbf{D}_{rr} [\mathbf{B}_{rr}^{\text{av}(\ell)}]$ 
14       $\mathcal{A}_{s(\ell)s(\ell)} = \mathcal{A}_{s(\ell)s(\ell)} + \chi_{F_r^{(\ell)}} [\mathbf{B}_{rs(\ell)}^{\text{av}(\ell)}]^\top \mathbf{D}_{rr} [\mathbf{B}_{rs(\ell)}^{\text{av}(\ell)}]$ 
15     else
16       Compute the diagonal contribution  $\mathbf{B}_{rr}^{\text{av}(\ell)}$ 
17        $\mathbf{b}_r = \mathbf{b}_r - [\mathbf{B}_{rr}^\nabla]^\top \mathbf{D}_{rr} [\mathbf{g}_r^{(\ell)}] + \chi_{F_r^{(\ell)}} [\mathbf{B}_{rr}^{\text{av}(\ell)}]^\top \mathbf{D}_{rr} [\mathbf{g}_r^{(\ell)}]$ 
18        $\mathcal{A}_{rr} = \mathcal{A}_{rr} - [\mathbf{B}_{rr}^\nabla]^\top \mathbf{D}_{rr} [\mathbf{B}_{rr}^{\text{av}(\ell)}] - [\mathbf{B}_{rr}^{\text{av}(\ell)}]^\top \mathbf{D}_{rr} [\mathbf{B}_{rr}^\nabla] + \chi_{F_r^{(\ell)}} [\mathbf{B}_{rr}^{\text{av}(\ell)}]^\top \mathbf{D}_{rr} [\mathbf{B}_{rr}^{\text{av}(\ell)}]$ 
19     end
20   end
21 end

```

---

**Remark 4.1** (Stability matrix in LDG method). *The implementation of the LDG method also involves a stability matrix  $S$ , and an additional vector  $\tilde{\mathbf{g}}$  associated with the Dirichlet boundary condition. More precisely, these terms are associated with the bilinear form and the linear functional*

$$\mathbf{s}_h(u_h, v_h) := \int_{\mathcal{F}_h^T} \eta_F [\![u_h]\!]_{\mathbf{N}} \cdot [\![v_h]\!]_{\mathbf{N}} \, dS + \int_{\mathcal{F}_h^D} \eta_F u_h v_h \, dS, \quad \tilde{g}_h(v_h) := \int_{\mathcal{F}_h^D} \eta_F g_D v_h \, dS.$$

*For the detailed definition of the penalty term  $\eta_F$  used in our code, we refer to [12, Eq. (4.26) in §4.3]. From a computational perspective, the matrix  $S$  has a natural compact stencil and is not affected by the choice of the weighted-average parameters. However, the presence of this additional matrix increases the computational cost w.r.t. the CDG method.* ■

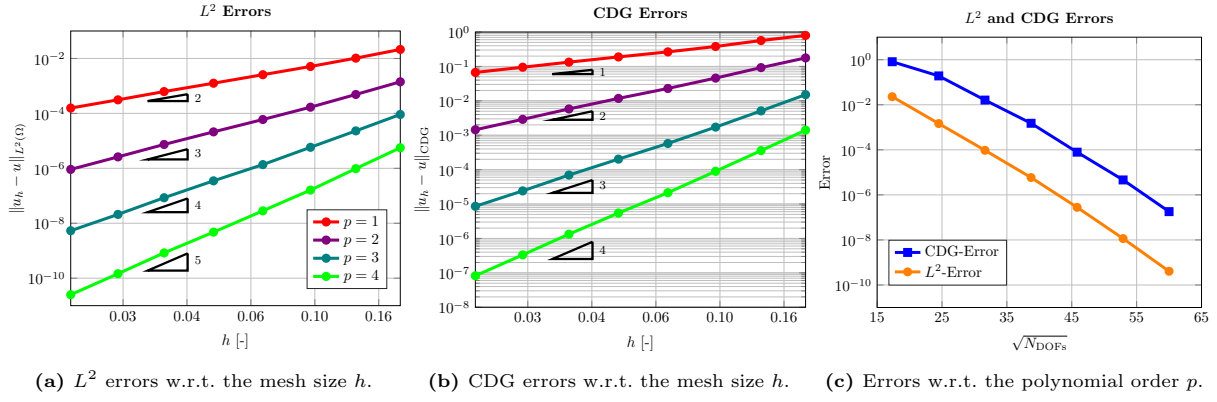


**Figure 2:** Computed errors in  $L^2$  norm (a) and CDG norm (b) w.r.t. the mesh size  $h$  and computed errors in  $L^2$  norm and CDG norm (c) w.r.t. the polynomial order  $p$ .

**Algorithm 2:** FAST ASSEMBLY OF THE LINEAR SYSTEM FOR THE LDG METHOD

---

```

1 for  $r = 1$  to  $\mathcal{N}_h^{\text{ele}}$  do
2   Compute  $\mathbf{M}_{rr}^{-1}$ ,  $\mathbf{D}_{rr}$ , and  $\mathbf{B}_{rr}^{\nabla}$ 
3   Set  $\mathbf{D}_{rr} = \mathbf{M}_{rr}^{-1} \mathbf{D}_{rr} \mathbf{M}_{rr}^{-1}$ 
4   Compute the diagonal blocks  $\mathbf{B}_{rr}^{\text{av}}$  and  $\mathbf{S}_{rr}$ , the off-diagonal blocks  $\mathbf{B}_{rs}^{\text{av}}$  and  $\mathbf{S}_{rs}$ , and the
      vectors  $\mathbf{b}_{f,r}$ ,  $\mathbf{g}_r$ , and  $\tilde{\mathbf{g}}_r$ 
5   Set  $\mathbf{B}_{rr} = \mathbf{B}_{rr}^{\nabla} + \mathbf{B}_{rr}^{\text{av}}$  and  $\mathbf{B}_{rs} = \mathbf{B}_{rs}^{\text{av}}$ 
6    $\mathcal{A}_{rr} = \mathcal{A}_{rr} + \mathbf{S}_{rr}$  and  $\mathbf{b}_r = \mathbf{b}_{f,r} + \tilde{\mathbf{g}}_r$ 
7   for  $i \in \mathcal{N}_K$  do
8      $\mathcal{A}_{ri} = \mathcal{A}_{ri} + \mathbf{S}_{ri}$ 
9   end
10  Set  $\mathcal{N}_{K_r}^{\text{loop}} = \mathcal{N}_{K_r}^{\text{out}}$  (for LDGw) or  $\mathcal{N}_{K_r}^{\text{loop}} = \mathcal{N}_{K_r}$  (for LDGf) a
11  for  $i \in \mathcal{N}_{K_r}^{\text{loop}}$  do
12    for  $j \in \mathcal{N}_{K_r}^{\text{loop}}$  do
13       $\mathcal{A}_{ij} = \mathcal{A}_{ij} + [\mathbf{B}_{ri}]^{\top} \mathbf{D}_{rr} [\mathbf{B}_{rj}]$ 
14    end
15    if  $\mathcal{F}_{K_r} \cap \mathcal{F}_h^{\mathcal{D}} \neq \emptyset$  then
16       $\mathbf{b}_r = \mathbf{b}_r + [\mathbf{B}_{ri}]^{\top} \mathbf{G}_r$ 
17    end
18  end
19 end

```

---

<sup>a</sup> $\mathcal{N}_{K_r}^{\text{out}}$  is defined in (2.7), and  $\mathcal{N}_{K_r}$  is the set neighbors of  $K_r$ .

## 5 Numerical experiments

In this section, we present some numerical tests to assess the accuracy and efficiency of the CDG method. In Section 5.1, we discuss the convergence of the CDG method. In Section 5.2, we compare the CDG computational efficiency with respect to that of the LDG and BR2 methods.

All numerical simulations in this section are based on the `lymph` library [1], implementing DG methods on polytopic meshes. The polygonal meshes are constructed using PolyMesher [32].

For the numerical tests in this section, we consider the space domain  $\Omega = (0, 1)^2$  and Dirichlet boundary conditions on  $\partial\Omega$  (namely,  $\Gamma_N = \emptyset$ ). Concerning the diffusion tensor, we consider  $\kappa = \mathbf{I}$ , where  $\mathbf{I}$  represents the identity matrix of size 2. We adopt the following manufactured exact solution  $u(x, y) = \sin(2\pi x) \cos(2\pi y)$ , and we compute the forcing term  $f$  and the boundary condition  $g_D$ , accordingly.

### 5.1 Convergence properties of CDG method

We perform a convergence test for uniform degrees of approximation  $p = 1, 2, 3, 4$  and regular Voronoi meshes, using, for each degree, eight different refinements with number of elements  $N_{\text{el}} = 100, 200, 400$ ,

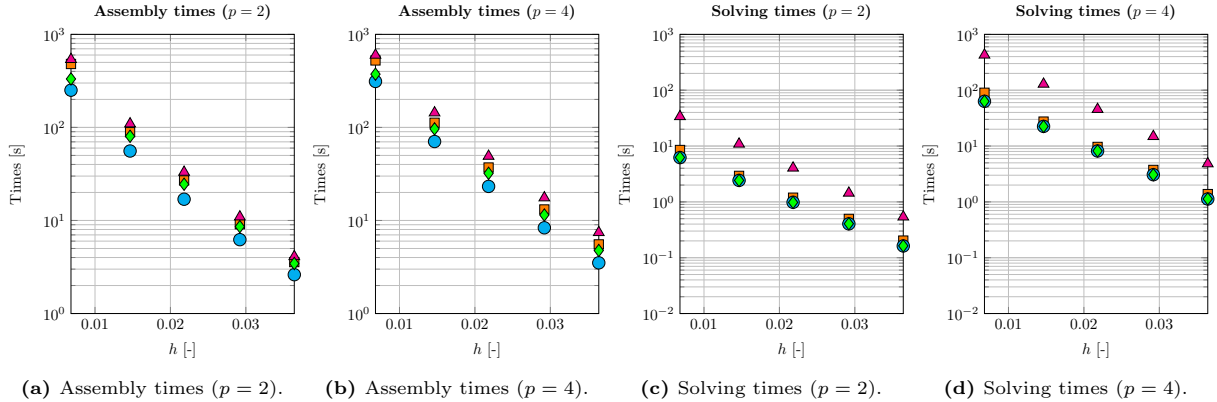


**Figure 3:** Comparison of computational times for the different methods (CDG, BR2, LDG<sub>w</sub>, and LDG<sub>f</sub>) and different polynomial orders ( $p = 2, 4$ ). The considered times are divided in assembly time (a–b) and solving time (c–d).

..., 12800. The weighted-average parameters  $\alpha_F$  and the parameter  $\gamma$  in Assumption 2.2 are set as  $\alpha_F = 1$  if  $\mathbf{n}_F \cdot (1, 0)^\top \geq 0$  (and  $\alpha_F = 0$  otherwise), and  $\gamma = 0.9$ .

In Figure 2a, we report the computed errors in  $L^2(\Omega)$  norm, and observe a decrease in the error with order  $\mathcal{O}(h^{p+1})$ . Moreover, in Figure 2b, the errors in the CDG norm show a convergence of order  $\mathcal{O}(h^p)$ . Finally, in Figure 2c, we report the errors in the CDG and  $L^2$  norms for the  $p$ -version of the method, namely, maintaining a fixed mesh of 100 elements ( $h \approx 0.1851$ ) and increasing the polynomial order  $p = 1, \dots, 7$ . We observe an exponential decay of the error of order  $\mathcal{O}(e^{-c\sqrt{N_{\text{DOFs}}}})$ .

## 5.2 Comparison between CDG, BR2 and LDG methods

As a second test case, we discuss the computational efficiency of the CDG method with respect to the BR2 and LDG methods. In particular, we discuss the LDG method by considering LDG<sub>f</sub> and LDG<sub>w</sub> versions separately. For LDG<sub>w</sub>, we have adopted the same choice of  $\alpha_F$  as for the CDG method, namely, we consider  $\alpha_F = 1$  if  $\beta_F = \mathbf{n}_F \cdot (1, 0)^\top \geq 0$  (and  $\alpha_F = 0$  otherwise). We test different polynomial degrees  $p = 2, 4$  and, for each degree, five different mesh Voronoi-type meshes with  $N_{\text{el}} = 3200, 6400, 12800, 25600, 51200$ . We first consider the assembly times according to Algorithms 1 and 2, for the CDG, BR2, and LDG methods. In Figures 3a and 3b, we report the assembly times computed for different polynomial degrees  $p = 2$  and  $p = 4$ . We observe that the CDG method provides a faster assembly compared to all the other methods. In particular, for the finest mesh with  $p = 4$ , the BR2 assembly requires approximately 19.55% more time than CDG. This is due to the double computations in the face integrals resulting from the choice  $\alpha_F = 1/2$ . Concerning the LDG methods, the assembly times are higher by approximately 67.95% (for LDG<sub>w</sub>) and 91.66% (for LDG<sub>f</sub>) than that of CDG. These large values are mostly due to the presence of the two nested loops over the neighbors, which also causes the larger stencil (see Algorithm 2).

In Figures 3c and 3d, we report the corresponding solving times for different polynomial degrees  $p = 2$  and  $p = 4$ . We employ the `backslash` operator as linear solver to ensure a fair comparison. The results show similar solving times for the BR2 and CDG methods, which can be attributed to their identical number of nonzero entries (see Table 1) and the same stencil (see Figure 4). Comparing these solving times with those of the LDG methods reveals significantly longer times for the latters. In particular, the LDG<sub>f</sub> method requires approximately 577.78% more time than CDG, while LDG<sub>w</sub> requires about 42.85% more. This is likely due to the much higher number of nonzero entries in the stiffness matrix  $\mathcal{A}$ , as reported in Table 1 and illustrated in Figure 4. On the other hand, the LDG matrices exhibit better conditioning than those of the CDG method. The 2-condition number  $\kappa_2(\mathcal{A})$  grows with the same order  $\mathcal{O}(h^{-2})$  for all the discussed methods.

## 5.3 Impact of the parameter $\chi_F$ for different types of mesh

In this section, we discuss the impact of the value of the parameter  $\chi_F$  on the convergence of the numerical solution and on the coercivity of the bilinear form associated with the CDG method. For this test, we consider four different types of mesh: structured triangular, Cartesian, Voronoi, and agglomerated meshes. In the latter, the agglomeration is performed using the MAGNET library [2].

Elements ( $h$ )	3200 (0.0337)	12800 (0.0172)	51200 (0.0086)	Elements ( $h$ )	3200 (0.0337)	12800 (0.0172)	51200 (0.0086)
<b>CDG</b>	$7.18 \times 10^4$ (197 280)	$2.75 \times 10^5$ (796 824)	$1.22 \times 10^6$ (3 202 596)	<b>CDG</b>	$3.93 \times 10^5$ (789 120)	$1.47 \times 10^6$ (3 187 296)	$6.42 \times 10^6$ (12 810 384)
<b>BR2</b>	$6.72 \times 10^4$ (197 280)	$2.55 \times 10^5$ (796 824)	$1.10 \times 10^6$ (3 202 596)	<b>BR2</b>	$3.47 \times 10^5$ (789 120)	$1.34 \times 10^6$ (3 187 296)	$5.72 \times 10^6$ (12 810 384)
<b>LDG<sub>w</sub></b>	$7.78 \times 10^4$ (257 742)	$3.03 \times 10^5$ (1 043 838)	$1.36 \times 10^6$ (4 200 642)	<b>LDG<sub>w</sub></b>	$3.71 \times 10^5$ (1 030 968)	$1.42 \times 10^6$ (4 175 352)	$6.16 \times 10^6$ (16 802 568)
<b>LDG<sub>f</sub></b>	$6.36 \times 10^4$ (533 268)	$2.53 \times 10^5$ (2 170 296)	$1.05 \times 10^6$ (8 757 702)	<b>LDG<sub>f</sub></b>	$2.85 \times 10^5$ (2 133 072)	$1.13 \times 10^6$ (8 681 184)	$4.75 \times 10^6$ (35 030 808)

(a) Condition number and nonzero entries of  $\mathcal{A}$  ( $p = 1$ ).(b) Condition number and nonzero entries of  $\mathcal{A}$  ( $p = 2$ ).

Elements ( $h$ )	3200 (0.0337)	12800 (0.0172)	51200 (0.0086)
<b>CDG</b>	$1.17 \times 10^6$ (2 192 000)	$4.86 \times 10^6$ (8 853 600)	$1.89 \times 10^7$ (35 584 400)
<b>BR2</b>	$1.05 \times 10^6$ (2 192 000)	$4.26 \times 10^6$ (8 853 600)	$1.76 \times 10^7$ (35 584 400)
<b>LDG<sub>w</sub></b>	$1.09 \times 10^6$ (2 863 800)	$4.20 \times 10^6$ (11 598 200)	$1.81 \times 10^7$ (46 673 800)
<b>LDG<sub>f</sub></b>	$8.23 \times 10^5$ (5 925 200)	$3.33 \times 10^6$ (24 114 400)	$1.36 \times 10^7$ (97 307 800)

(c) Condition number and nonzero entries of  $\mathcal{A}$  ( $p = 3$ ).

Elements ( $h$ )	3200 (0.0337)	12800 (0.0172)	51200 (0.0086)
<b>CDG</b>	$2.78 \times 10^6$ (4 932 000)	$1.25 \times 10^7$ (19 920 600)	$4.87 \times 10^7$ (80 064 900)
<b>BR2</b>	$1.05 \times 10^6$ (4 932 000)	$4.26 \times 10^6$ (19 920 600)	$1.76 \times 10^7$ (80 064 900)
<b>LDG<sub>w</sub></b>	$2.68 \times 10^6$ (6 443 550)	$5.25 \times 10^6$ (12 976 200)	$4.46 \times 10^7$ (105 016 050)
<b>LDG<sub>f</sub></b>	$1.97 \times 10^6$ (13 331 700)	$8.02 \times 10^6$ (54 257 400)	$3.30 \times 10^7$ (218 942 550)

(d) Condition number and nonzero entries of  $\mathcal{A}$  ( $p = 4$ ).

**Table 1:** Condition number (first row in each cell) and nonzero entries of  $\mathcal{A}$  (second row in each cell) for the different methods (CDG, BR2, LDG<sub>w</sub>, and LDG<sub>f</sub>) and for different polynomial orders ( $p = 1, 2, 3, 4$ ).

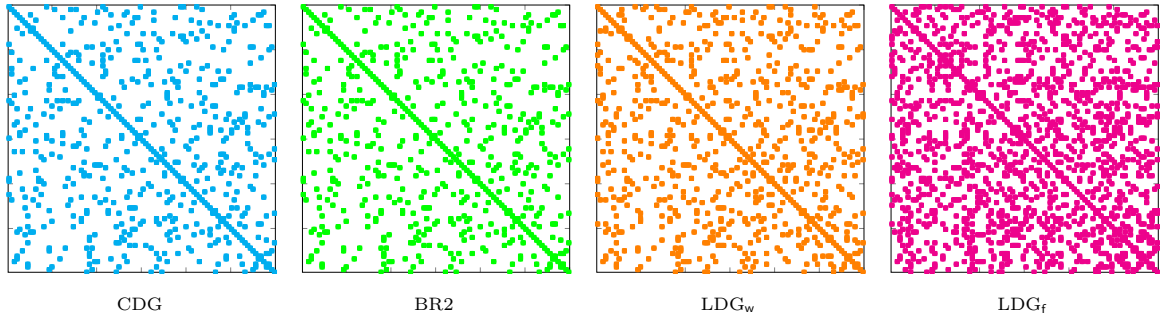


**Figure 4:** Comparison of sparsity patterns for the different methods (CDG, BR2, LDG<sub>w</sub>, and LDG<sub>f</sub>) with a mesh of 100 elements and polynomial degree  $p = 1$ .

For each type of mesh, we construct a sequence of refinements that we use to perform a convergence test with a fixed polynomial degree  $p = 4$ . In particular, we consider three different choices of  $\chi_F$ , first as in Assumption 2.2, and then fixing it as a constant, namely  $\chi_F = 1$  or  $\chi_F = 0.1$  for all facets  $F \in \mathcal{F}_h^I \cup \mathcal{F}_h^D$ . In Figure 5, we report the errors in both the  $L^2(\Omega)$  norm (see Figures 5a–5c) and the CDG norm (see Figures 5d–5f). We observe monotone convergence with the correct order for all mesh types only for the choice of  $\chi_F$  in Assumption 2.2 (Figures 5a and 5d). On the contrary, the constant choice  $\chi_F = 1$  causes loss of monotone convergence in meshes with a larger number of faces per element, namely the Voronoi and agglomerated meshes (Figures 5b and 5e). Finally, a significant loss of the convergence rates is observed for the choice  $\chi_F = 0.1$  also for the Cartesian grids (Figures 5c and 5f). No significant changes are observed for the triangular mesh in terms of convergence rates; however, the errors are one order larger for  $\chi_F = 0.1$  than for the other cases.

To analyze the reasons for the loss of convergence, we plot the minimum eigenvalue of the matrix  $\mathcal{A}$  for the different mesh types. In particular, we consider a coarse mesh ( $\sim 100$  elements) with  $p = 1$  and  $p = 4$  and a fine mesh ( $\sim 1000$  elements) with  $p = 1$ . We report the results in Figure 6, where we observe that eigenvalue positivity depends on the choice of  $\chi_F$ .

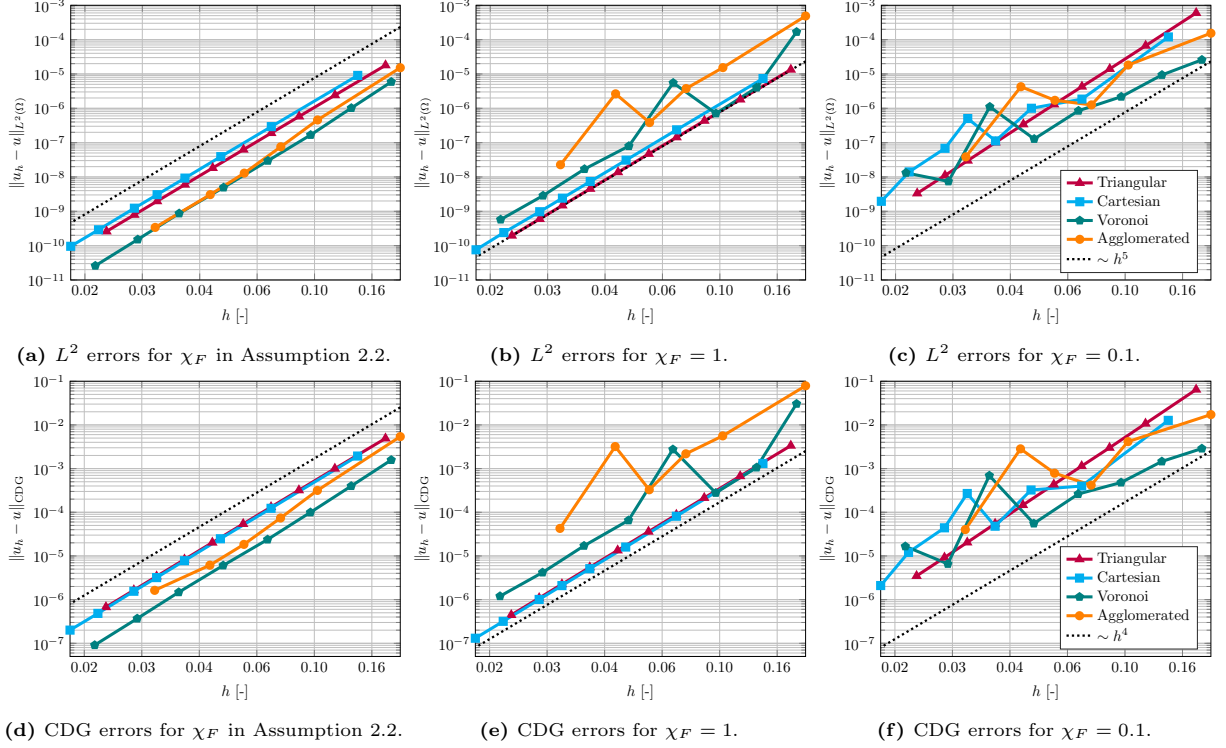


**Figure 5:** Computed errors in  $L^2(\Omega)$  norm (a-c) and CDG norm (d-f) w.r.t. the mesh size  $h$  and for different mesh types. The errors have been computed both considering  $\chi_F$  as in Assumption 2.2 (left),  $\chi_F = 1$  (center), and  $\chi_F = 0.1$  (right).

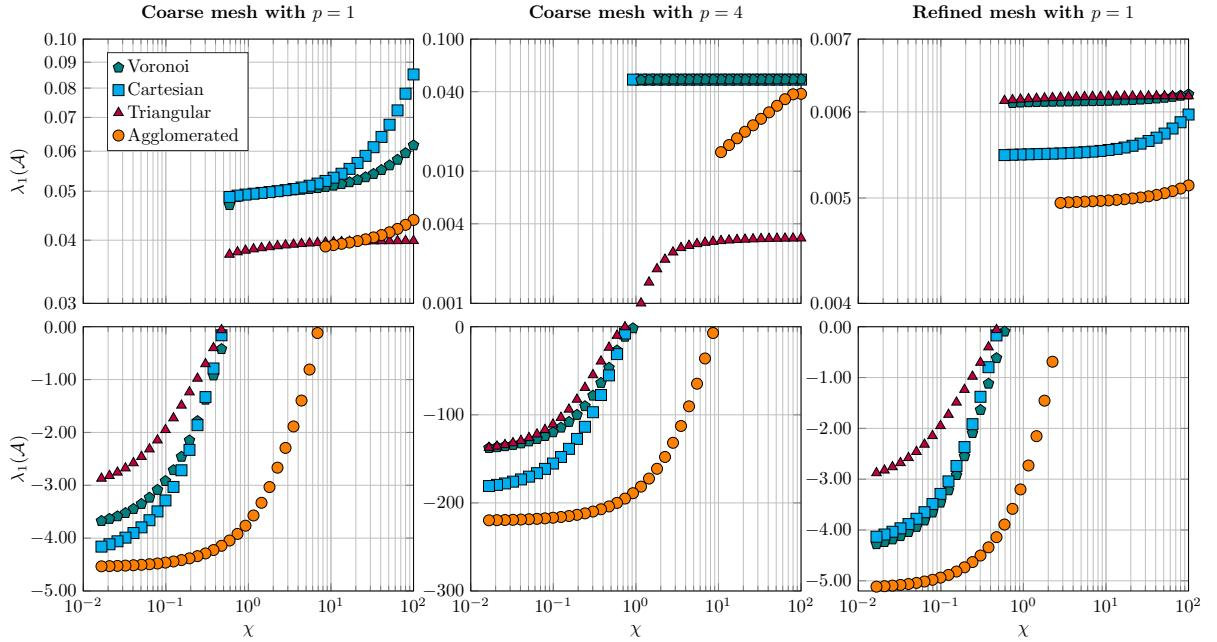


**Figure 6:** Minimum eigenvalue of the matrix  $\mathcal{A}$  for different meshes and polynomial orders: coarse mesh with  $p = 1$  (left), coarse mesh with  $p = 4$  (center), and fine mesh with  $p = 1$  (right). Each plot is divided into an upper panel where the eigenvalue is positive in log scale and a lower panel for the negative values in normal scale.

In particular,  $\chi_F$  needs to be large enough to ensure coercivity of the problem. The agglomerated mesh, where each element has a large number of facets, requires a larger  $\chi_F$  to maintain coercivity. Indeed, a refinement of the agglomerated mesh that reduces the number of facets restores eigenvalue positivity for smaller values of  $\chi_F$ . Coherently, no significant changes occur for the other mesh types upon refinement. Moreover, the minimum value of  $\chi$  that produces a positive-definite stiffness matrix depends just mildly on the degree of approximation  $p$ . However, for values of  $\chi$  below this threshold,

substantially larger negative values are obtained.

#### 5.4 Choice of $\alpha_F$ in the $p$ -variable case

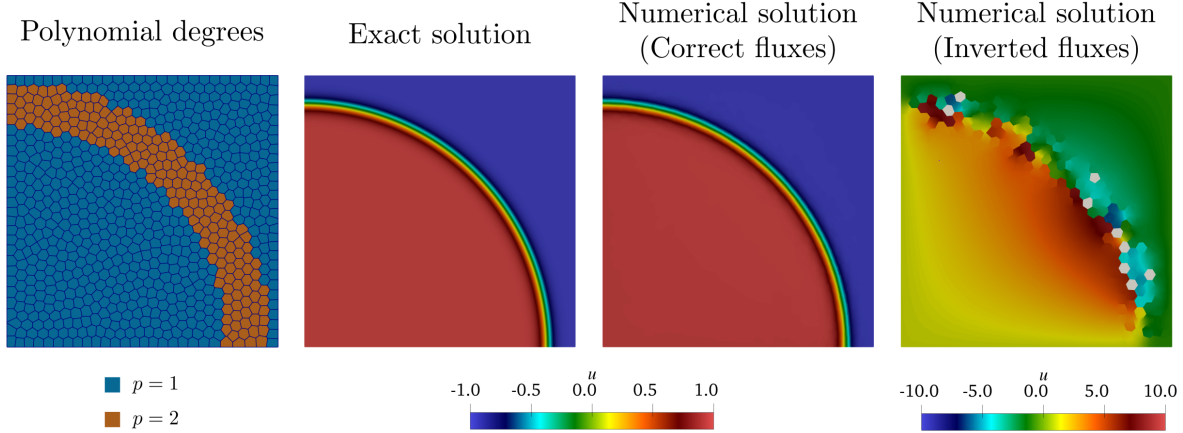


**Figure 7:** Computational mesh and polynomial degrees distribution (first figure), exact solution of the problem (second figure), and numerical solutions computed with the correct fluxes (third figure) and with the inverted ones (fourth figure). In the latter, the color gray corresponds to `NaN` values

In this test case, we study the impact of Assumption 2.1 on the stability of the numerical method for variable degrees of approximation. We perform a simulation on the domain  $\Omega = (0, 1)^2$ , using a regular Voronoi mesh of 800 elements (see Figure 7, leftmost panel). We consider the problem with exact solution  $u(x, y) = \tanh(-20(x^2 + y^2 - 0.8))$  and a variable polynomial degree with  $p = 2$  in the region of highest gradient, and  $p = 1$  elsewhere, as illustrated in Figure 7 (first panel).

In Figure 7 (third panel), we report the numerical solution computed with  $\alpha_F$  chosen as in Assumption 2.1 (“correct fluxes”), which provides an accurate approximation. Moreover, we report the numerical solution obtained by choosing “inverted fluxes”, namely by choosing  $\alpha_F$  such that the trace of  $\sigma_h^F$  is taken from the lowest-order mesh element in the numerical fluxes. Figure 7 (rightmost panel) exhibits a severe degradation of the approximation, resulting from the ill-conditioning of the linear system.

## 6 Concluding remarks

In this work, we have presented theoretical and computational aspects of the  $hp$ -version of the CDG method on polytopal meshes. In particular, we proved the well-posedness of the scheme and derived *a priori* error estimates. In addition, we introduced efficient strategies to implement the CDG, LDG, and BR2 methods within a common framework. The numerical experiments validated the theory and discussed the advantages of the CDG method in terms of computational cost and stencil compactness, making it particularly appealing for applications involving polytopal meshes. Possible future research directions include the extension to more complex problems, and the development of  $hp$ -adaptivity driven by suitable *a posteriori* error estimators.

## Acknowledgments

This research was partially supported by the European Union (ERC Synergy, NEMESIS, project number 101115663). Views and opinions expressed are, however, those of the authors only and do not necessarily reflect those of the EU or the ERC Executive Agency. This research was funded in part by the Austrian Science Fund (FWF) project 10.55776/F65. The authors are members of the INdAM-GNCS group. The present research is part of the activities of Dipartimento di Eccellenza 2023-2027 (Dipartimento di Matematica, Politecnico di Milano).

## References

- [1] P. F. Antonietti, S. Bonetti, M. Botti, M. Corti, I. Fumagalli, and I. Mazzieri. `1ymph`: discontinuous polytopal methods for Multi-PHysics differential problems. *ACM Trans. Math. Softw.*, 51(1):3:1–3:22, 2025.
- [2] P. F. Antonietti, M. Caldana, I. Mazzieri, and A. Re Fraschini. Magnet: an open-source library for mesh agglomeration by graph neural networks. *Eng. Comput.*, 41(6):4825–4850, 2025.
- [3] P. F. Antonietti, M. Corti, and G. Martinelli. Polytopal mesh agglomeration via geometrical deep learning for three-dimensional heterogeneous domains. *Math. Comput. Simul.*, 241:335–353, 2026.
- [4] D. N. Arnold. An interior penalty finite element method with discontinuous elements. *SIAM J. Numer. Anal.*, 19(4):742–760, 1982.
- [5] D. N. Arnold, F. Brezzi, B. Cockburn, and L. D. Marini. Unified analysis of discontinuous Galerkin methods for elliptic problems. *SIAM J. Numer. Anal.*, 39(5):1749–1779, 2001/02.
- [6] F. Bassi, L. Botti, A. Colombo, D. A. Di Pietro, and P. Tesini. On the flexibility of agglomeration based physical space discontinuous Galerkin discretizations. *J. Comput. Phys.*, 231(1):45–65, 2012.
- [7] F. Bassi, S. Rebay, M. Savini, G. Mariotti, and Pedinotti. A high-order accurate discontinuous finite element method for inviscid and viscous turbomachinery flows. In *2-nd European Conference on Turbomachinery Fluid Dynamics and Thermodynamics*, pages 99–108. Technologisch Instituut, Antwerpen, Belgium, 1997.
- [8] L. Beirão da Veiga, F. Brezzi, A. Cangiani, G. Manzini, L. D. Marini, and A. Russo. Basic principles of virtual element methods. *Math. Models Methods Appl. Sci.*, 23(1):199–214, 2013.
- [9] S. Brdar, A. Dedner, and R. Klöfkorn. Compact and stable discontinuous Galerkin methods for convection-diffusion problems. *SIAM J. Sci. Comput.*, 34(1):A263–A282, 2012.
- [10] F. Brezzi, G. Manzini, D. Marini, P. Pietra, and A. Russo. Discontinuous Galerkin approximations for elliptic problems. *Numer. Methods Partial Differential Equations*, 16(4):365–378, 2000.
- [11] A. Cangiani, Z. Dong, and E. H. Georgoulis.  $hp$ -version discontinuous Galerkin methods on essentially arbitrarily-shaped elements. *Math. Comp.*, 91(333):1–35, 2021.
- [12] A. Cangiani, Z. Dong, E. H. Georgoulis, and P. Houston. *hp-version discontinuous Galerkin methods on polygonal and polyhedral meshes*. SpringerBriefs Math. Cham: Springer, 2017.
- [13] A. Cangiani, E. H. Georgoulis, and P. Houston.  $hp$ -version discontinuous Galerkin methods on polygonal and polyhedral meshes. *Math. Models Methods Appl. Sci.*, 24(10):2009–2041, 2014.
- [14] P. Castillo. Performance of discontinuous Galerkin methods for elliptic PDEs. *SIAM J. Sci. Comput.*, 24(2):524–547, 2002.
- [15] P. Castillo. Stencil reduction algorithms for the local discontinuous Galerkin method. *Internat. J. Numer. Methods Engrg.*, 81(12):1475–1491, 2010.
- [16] P. Castillo, B. Cockburn, I. Perugia, and D. Schötzau. An a priori error analysis of the local discontinuous Galerkin method for elliptic problems. *SIAM J. Numer. Anal.*, 38(5):1676–1706, 2000.
- [17] P. Castillo and F. A. Sequeira. Computational aspects of the local discontinuous Galerkin method on unstructured grids in three dimensions. *Math. Comput. Modelling*, 57(9-10):2279–2288, 2013.
- [18] B. Cockburn and C.-W. Shu. The local discontinuous Galerkin method for time-dependent convection-diffusion systems. *SIAM J. Numer. Anal.*, 35(6):2440–2463, 1998.
- [19] D. A. Di Pietro and J. Droniou. *The hybrid high-order method for polytopal meshes. Design, analysis, and applications*, volume 19 of *MS&A, Model. Simul. Appl.* Cham: Springer, 2020.
- [20] D. A. Di Pietro, A. Ern, and S. Lemaire. An arbitrary-order and compact-stencil discretization of diffusion on general meshes based on local reconstruction operators. *Comput. Methods Appl. Math.*, 14(4):461–472, 2014.

- [21] S. Gómez, C. Perinati, and P. Stocker. Inf-sup stable space-time Local Discontinuous Galerkin method for the heat equation. *J. Sci. Comput.*, 106:Paper No. 22, 2026.
- [22] D. P. Hewett. Piecewise polynomial approximation on non-Lipschitz domains. [arXiv:2511.22628](https://arxiv.org/abs/2511.22628), 2025.
- [23] X. Huang and J. Huang. The compact discontinuous Galerkin method for nearly incompressible linear elasticity. *J. Sci. Comput.*, 56(2):291–318, 2013.
- [24] H. Liu and J. Yan. The direct discontinuous Galerkin (DDG) methods for diffusion problems. *SIAM J. Numer. Anal.*, 47(1):675–698, 2008/09.
- [25] Y. Pan and P.-O. Persson. Agglomeration-based geometric multigrid solvers for compact discontinuous Galerkin discretizations on unstructured meshes. *J. Comput. Phys.*, 449:Paper No. 110775, 12, 2022.
- [26] W. Pazner. Efficient low-order refined preconditioners for high-order matrix-free continuous and discontinuous Galerkin methods. *SIAM J. Sci. Comput.*, 42(5):A3055–A3083, 2020.
- [27] J. Peraire and P.-O. Persson. The compact discontinuous Galerkin (CDG) method for elliptic problems. *SIAM J. Sci. Comput.*, 30(4):1806–1824, 2008.
- [28] I. Perugia and D. Schötzau. An  $hp$ -analysis of the local discontinuous Galerkin method for diffusion problems. *J. Sci. Comput.*, 17(1-4):561–571, 2002.
- [29] D. Schötzau, C. Schwab, and A. Toselli. Mixed  $hp$ -DGFEM for incompressible flows. *SIAM J. Numer. Anal.*, 40(6):2171–2194, 2002.
- [30] S. J. Sherwin, R. M. Kirby, J. Peiró, R. L. Taylor, and O. C. Zienkiewicz. On 2D elliptic discontinuous Galerkin methods. *Internat. J. Numer. Methods Engrg.*, 65(5):752–784, 2006.
- [31] E. M. Stein. *Singular integrals and differentiability properties of functions*, volume 30 of *Princeton Math. Ser.* Princeton University Press, Princeton, NJ, 1970.
- [32] C. Talischi, G. H. Paulino, Anderson P., and Ivan F. M. Menezes. **PolyMesher**: a general-purpose mesh generator for polygonal elements written in Matlab. *Struct. Multidiscip. Optim.*, 45(3):309–328, 2012.
- [33] T. Warburton and J. S. Hesthaven. On the constants in  $hp$ -finite element trace inverse inequalities. *Comput. Methods Appl. Mech. Engrg.*, 192(25):2765–2773, 2003.
- [34] T. P. Wihler. *Discontinuous Galerkin FEM for elliptic problems in polygonal domains*. PhD thesis, ETH Zurich, 2002.
- [35] X. Ye, S. Zhang, and P. Zhu. Development of a LDG method on polytopal mesh with optimal order of convergence. *J. Comput. Appl. Math.*, 410:Paper No. 114179, 10, 2022.